Synthesis, NMR, IR, Raman spectra and DFT calculations of 1-octyl-1,4-diazabicyclo [2.2.2] octan-1-ium bis(trifluoromethylsulfonyl)imide

Boumediene Haddad, Silvia Antonia Brandán, Bekhaled Fetouhi, Annalisa Paolone, Mostefa Boumediene, Didier Villemin, Mustapha Rahmouni, Serge Bresson

Synthesis, NMR, IR, Raman spectra and DFT calculations of 1-octyl-1,4-diazabicyclo [2.2.2] octan-1-ium bis(trifluoromethylsulfonyl)imide

Boumediene Haddad[1,2,*], Silvia Antonia Brandán[3],BekhaledFetouhi[4,5],Annalisa Paolone[6] , MostefaBoumediene[1], Didier Villemin[2], Mustapha Rahmouni[5], Serge Bresson[7]

[1] Department of Chemistry, Dr. Moulay Tahar University of Saida, 20000 Saida, Algeria.

[2] LCMT, ENSICAEN, UMR 6507 CNRS, University of Caen, 6 bd Ml Juin, 14050 Caen, France.

[3] Cátedra de Química General, Instituto de Química Inorgánica, Facultad de Bioquímica. Química y Farmacia, Universidad Nacional de Tucumán, Ayacucho 471, (4000) San Miguel de Tucumán, Tucumán, Argentina

[4] Faculty of Natural and Life Sciences, University of Tiaret, BP78 ZaarouraTiaret 14000, Algeria.

[5] Synthesis and Catalysis Laboratory LSCT, Tiaret University, Tiaret, Algeria

[6] CNR-ISC, U.O.S. La Sapienza, Piazzale A. Moro 5, 00185 Roma, Italy

[7] UP Transformations & Agro-Ressources, InstitutPolytechniqueUniLaSalle, SFR Condorcet 3417, BP 30313, F-60026 Beauvais, France

*Corresponding author: Tel.: +213676802567

E-mail :haddadboumediene@yahoo.com (Prof. Dr. HADDAD Boumediene).

ABSTRACT

In this study, a novel [C_8DABCO$^+$][$(CF_3SO_2)_2N^-$] ionic liquid (IL) was prepared by an alkylation reaction and then characterized it by experimental ^{1}H-, ^{13}C-, and ^{19}F-NMR, IR and Raman spectroscopies together with B3LYP/6-311G** calculations in gas phase and aqueous solution to confirm its structure. DSC and TGA measurements show that it can be classified as a thermally stable ionic liquid. Three different structures (I), (II) and (III) were proposed for the IL with *Cis* and *Trans* positions of CF_3 groups of anion evidencing better correlations among experimental and predicted spectra for structure (III). Strong S-O···H interactions were predicted in the gas phase while in solution the C-F···H distance is shorter (2.654 Å) than the S-O···H ones (2.827 Å). The analysis of MK charges reveals the presence of positive charges on quaternary N23 atoms both in vaccum and in solution; conversely positive Mulliken charges reside on O49 and O50 in the gas phase, while negative ones are found in solution. Molecular Electrostatic potential (MEP) surfaces support the electrophilic sites on quaternary N23 while the nucleophilic sites are observed on O, N and F atoms of the anion. NBO and AIM calculations reveal the characteristics of cation-anion interactions in the two media, as supported by the different *f(νN-C)*, *f(νSO$_2$)*, *f(δSO$_2$)* and *f(δCH$_2$)* force constants values. Gap values suggest that [C_8DABCO$^+$][$(CF_3SO_2)_2N^-$] is less reactive than [C_8DABCO$^+$][Br^-] while the characteristics of frontier orbitals justify the cation-anion interactions and support the important role of 1,4-diazabicyclo[2.2.2]octane (DABCO) in the properties of [C_8DABCO$^+$][$(CF_3SO_2)_2N^-$] IL in both media. The complete assignments of 174 vibration modes expected for [C_8DABCO$^+$][$(CF_3SO_2)_2N^-$] IL are reported together with the scaled force constants.

KEYWORDS:1-octyl-1,4-diazabicyclo [2.2.2] octan-1-ium; bis(trifluoromethanesulfonyl)imide; NMR;Raman spectroscopy; IR spectroscopy; TGA; DTA; DFT calculations.

1. Introduction

Ionic liquids are salts structurally composed of a sizeable, charge diffuse, organic cation and an inorganic/organic anion [1-2]. Due to a number of advantageous properties, ionic liquids have attracted largeattention as solvents, also because of their low vapor pressure and flammability [3-4].Different cation-anion combinations can in principle lead to the synthesisof new andnumerous organic salts [5].To date, ionic liquids (ILs) are classified and used as biosolvents in several areas to avoid serious environmental impacts[5].In the last decade, also multivalent and bicyclic cations have been used to form ionic liquids,useful forbiologicalapplications[6-7]. It is possible to form symmetrical or asymmetrical ILs from heterobicyclic compound, like1-alkyl-4-aza-1-azaniabicyclo [2.2.2] octyl ammonium (DABCO), containing different substituents, that are commonly known as DABCO-based ionic liquids. These compounds can be applied as building units of excellent molecular ferroelectrics and are very useful as solvents for organic synthesis [8-9]. 1,4-diazabicyclo[2.2.2]octane (DABCO) ILscontributed to populate an emerging variety of ionic liquids by introducing chemical modifications of cations and anions [10-13], and are excellent candidates to prepare new ionic liquids [14].The influence of structural parameters such as, the type of the cation and the nature of the anion, the length of the side chain on the physicochemical properties of ILs has been partially studied [15]. Ishtiaq et al. [16] investigated the catalytic efficiency in catalyzing the organic reactionsof 1,4-diazabicyclo[2.2.2]octane (DABCO)-based ionic liquids with fluoride anions. Their results indicated that DABCO-F can be successfully utilized in organic syntheses by their dual role as ionic liquid and as a catalyst. With the same objective, Safari et al [17] reported the structural and thermal properties of $[C4(H\text{-}DABCO)_2][HSO_4]_4$ and showed the application as an efficient, acidic catalyst for the acceleration of the synthesis of 2H-indazolo [2,1-b] phthalazine-trione and [1,2,4] triazoloquinazolinone derivatives. Very recently, we have investigated the molecular structure and the vibrational properties of 1-octyl-1,4-diazabicyclo [2.2.2] octan-1-ium coupled with the bromide and hexafluorophosphate anions by using NMR, IR and Raman spectroscopy. The results indicated the cation-anion interactions play an important role on the structural, thermal, electronic, topological and vibrational properties of 1-octyl-1,4-diazabicyclo [2.2.2] octan-1-ium ILs [18-19]. To the best of our knowledge, manydetails of structures and structural, thermal, electronic, topological and vibrational propertiesand their relationship with microscopic properties are not covered yet by the literaturedue to the impossibility of obtaining crystals for structural determination using X-ray diffraction. In this context, to elucidate the structure of a new ionic liquid, its

experimental characterizations by means of 1H-, 13C-, and 19F-NMR, mass, infrared Raman and ultraviolet spectroscopies must be combined with theoretical calculations in order to confirm the proposed structure by means of comparisons of its corresponding spectra [2,17-21]. In the present study, the structure and properties of 1-octyl-1,4-diazabicyclo [2.2.2] octan-1-ium bis- (trifluoromethylsulfonyl)imideionic liquid,[C_8DABCO^+][$(CF_3SO_2)_2N^-$],are studied and analyzed combining the ^{1}H-NMR, ^{13}C-NMR, ^{19}F-NMR, infraredand Raman spectra with B3LYP/6-31G* and B3LYP/6-311G** calculations. Also, the experimental thermal properties of new ionic liquid were also evaluatedtogether with its structural and vibrational, topological, electronic properties and reactivities in the gas phase and aqueous solution. Here, complete assignments of vibrational spectra and the force constants of anion and cation were reported.

2. Experimental

2.1. Materials and methods

2.1.1. Chemicals for Synthesis

Chemicals and reagents, i.e 1,4-diazabicyclo [2.2.2] octane (DABCO) (>99%), 1-bromooctane (98%) and lithiumbis(trifluoromethanesulfonyl)imide ([Li^+][$(CF_3SO_2)_2N^-$]),were of analytical grade and procured from Fluka. All solvents, such as ethyl acetate, di-ethyl- ether and deionized H_2O, were purchased from Sigma Aldrich.

The general synthesis of the studied ionic liquid namely 1-octyl-1,4-diazabicyclo [2.2.2] oc-tan-1-ium bis(trifluoromethanesulfonyl)imide is illustrated in Scheme 1.

Synthesis of 1-octyl-1,4-diazabicyclo [2.2.2] octan-1-ium Bromide [C_8DABCO^+][Br^-]:

The synthesis procedure was carried out as reported in our recent papers [18],1,4-diazabicyclo [2.2.2] octane (9.95 g, 88,7 mmol)) and 1-bromooctane(18g, 93,2 mmol)were dissolved in AcOEt (125 ml) before being stirred at room temperature (25 °C) for 24 h. The obtained [$DABCO8^+$][Br^-] was evaporated under vacuum to remove AcOEt and then washed with diethyl ether (100 mL) to give the 1-octyl-1,4-diazabicyclo [2.2.2] octan-1-ium Bromide [$DABCO8^+$][Br^-] as a yellowish solid (16,91g). The yield of this reaction was 57%.

Synthesis of 1-octyl-1,4-diazabicyclo [2.2.2] octan-1-ium bis(trifluoromethanesulfonyl)imide [C_8DABCO^+][$(CF_3SO_2)_2N^-$]:

The synthesis was performed at room temperature (25 °C)through a metathesis reaction:2.88 g of lithium bis(trifluoromethanesulfonyl)imide [Li^+][$(CF_3SO_2)_2N^-$] dissolved in 20 mL of deionized water were added toa flask containing 3g of [$DABCO8^+$][Br^-] dissolved in 20 mL of deionized water. The mixture consisted of two separate phases: the ionic liquid at the

bottom and an aqueous solution at the top. The former was separated from the latter by centrifugation (3000 rpm) for 60 s. After isolation, the obtained $[C_8DABCO^+][(CF_3SO_2)_2N^-]$ was dried in vacuum at 100 °C for 2 h, yielded 59% of colorless to pale yellow liquid product. The ionic liquid was dried in phosphorus pentoxide, P_2O_5, to remove residual water. The determination of water content was performed by coulometric Karl Fischer titration using a Metrohm 831 and was found to be lower than420 ppm.The NMR analysis (^1H, ^{13}C, ^{19}F-NMR) of the $[C_8DABCO^+][(CF_3SO_2)_2N^-]$ IL is described in Section NMR Spectroscopic study.

Scheme 1.General synthesis of $[C_8DABCO^+][(CF_3SO_2)_2N^-]$.

2.2.2. NMR measurements

The NMR analysis includes ^1H (500 MHz), ^{13}C (125.75 MHz), ^{19}F (470.62 MHz) and ^{31}P-NMR (202.47 MHz) spectra thatwere recorded in $CDCl_3$ and DMSO-d_6 solutions by using a Bruker DRX 500 MHz spectrometer. The chemical shifts (δ) are given in ppm and referenced to the internal solvent signal namely TMS, $CFCl_3$ and H_3PO_4, respectively. The coupling constants (J) are expressed in Hertz (Hz).

2.2.3. FT-Raman andFT-infraredmeasurements

The FT-Raman spectrum of $[C_8DABCO^+][(CF_3SO_2)_2N^-]$ was acquired in the wavenumber range 4000-45 cm^{-1} with a resolution of 1 cm^{-1},adding 128 scans at room temperature bya Vertex 70-RAM II Bruker FT-Raman spectrometer. Additionally, the FT-IR spectrum of $[C_8DABCO^+][(CF_3SO_2)_2N^-]$ in the liquid state was recorded between 4000 and 600 $cm^{-1}$with a spectral resolution of 1 cm^{-1}adding 64 scans on a Bruker Vertex II-70 Spectrometer (Bruker Analytical, Slough, United Kingdom).

2.2.4. Thermal characterization

In the temperature ranges[-80 to 200 °C] and [25 to 700 °C] respectively, DSC and TGA measurements were collected by means of a Mettler Toledo DSC3 and a Setaram Setsys Evolution 1200 TGA system in an inert (argon) helium flux of 60 mL/min. Experiments in scanning mode at 5 or 10 °C/min were conducted for DSC and TGA, respectively on heating. The initial mass of the samples for the two types of experiments was in the range of 15 mg.

2.3. Computational details

Two initial structures of $[C_8DABCO^+][(CF_3SO_2)_2N^-]$ ionic liquid were theoretically modelled taking into account the previously optimized structures of cation $[C_8DABCO^+]$ and anion

[$(CF_3SO_2)_2N^-$] by using B3LYP/6-311++G** calculations with the *GaussView* program [20-23]. In the structure (I) the CF_3 groups of anion has *Cis* position, while in (II) it has the *Trans* one. Both IL structures were optimized with the B3LYP/6-31G* level of theory and the two are reported in **Figure 1**. Then, when the theoretical calculations were performed with the B3LYP/6-311G** method another different structure (III) of lower energy was optimized. **Figure 2** shows the optimized structure (III) with the CF_3 groups of anion in *Trans* position. Therefore, the three structures were optimized in gas phase and aqueous solution by using the hybrid B3LYP method with the Gaussian 09 program [23-26]. Only in (I), the CF_3 groups of anion presents *Cis* position while in (II) and (III) they are in *trans* position because these are the most stable positions with lower energies. The three structures show different S47-O49⋯H16 and C53-F60⋯H29 interactions with distances between 2.077 and 3.388 Å (See Figures1 and 2) but in (III) the distances are around 2.189 and 2.261 Å while the values in (I) are between 2.077 and 2.250Å. Although the distances are slightly smaller for (I), here we present in Table 5 the values only for structure (III) because it is the one that presents the best correlations between the experimental spectra, as was later mentioned in the Results and Discussion section. The characteristics of the reached stationary points were checked by positive frequencies. Here, it is very important to mention that enhanced correlations among the experimental NMR, IR and Raman spectra with the predicted ones were obtained for the structure (III) and, for this reason,only this structure was considered to predict the properties of new IL by using the B3LYP/6-311G** method. Atomic charges, stabilization energies, bond orders, molecular electrostatic potentials and topological properties were predicted for IL in both media by using natural bond orbital (NBO) and atoms in molecules (AIM) calculations [27-30]. Changes in volumes were analysed with the Moldraw program [31]. The harmonic force fields of IL in the two media were computed with the scaled quantum mechanical force field (SQMFF) methodology and the Molvib program taking into account the normal internal coordinates for cation and anion and transferable scaling factors [32-34].Improvedrelationshipswere obtained transforming the predicted Raman spectra fromactivities to intensities [35]. The NMR chemical shifts were predicted by using a gage-invariant linear combination of atomic orbitals (LCAO) method [36]. Reactivities and behaviors of IL and its cation and anion in both media were predicted by using the frontier orbital and clasical equations [18,19,37-39]. Finally, the electronic spectrum of IL in aqueous solution was predicted and compared with the corresponding to cation and anion in the same mediumby using the time-dependent DFT calculations (TD-DFT) with the Gaussian 09 program [23].

3. Resultsanddiscussion

3.1. NMR spectral analysis

Due to that the structure of synthesised $[C_8DABCO^+][(CF_3SO_2)_2N^-]$ IL was not experimentally determined by X-ray diffraction, the confirmation of it was performed by comparisons between the experimental ^1H, ^{13}C and ^{19}F-NMR spectrawith the corresponding theoretical predicted for those three optimized structures by using the root-mean-square deviation (RMSD) values. These spectral analyses of NMR measures are useful to determine the structure of organic compounds and to identify the chemical environment of each atom; it is a very reliable method to verify the molecular structure of compounds. Therefore, these spectral data are given below.

^{1}H–NMR ($CDCl_3$) δ_H(ppm) = 3.25-3.19 (t,^{3}J=7.4 Hz,6H), 3.15-3.12 (t,^{3}J=8 Hz,2H), 3.08 (s,6H), 1.64-1.63 (m, 2H), 1.58-1.52 (m, 2H),1.27-1.22 (m, 2H), 1.19 (m, 6H), 0.82-0.79 (t,^{3}J=7.2 Hz,3H).

^{13}C–NMR ($CDCl_3$) δ_C(ppm) =120.81 ,118.60, 64.88, 52.57, 44.98, 31.59, 28.85, 25.92, 22.33, 21.64, 13.74.

^{19}F–NMR (DMSO-d_6) δ_F ppm= −78.93 (s, [NT**f**$_2^-$]).

In **Figures 3a, 3b and 3c** we report the experimental ^1H, ^{13}C and ^{19}F-NMR spectra of IL in $CDCl_3$, respectively while in **Tables 1, 2** and **3** the experimental ^1H,^{13}C and^{19}F-NMR chemical shifts are shown compared with the calculated ones for the three structures by using the Gauge-Independent Atomic Orbital (GIAO) method, the B3LYP level of theory and the 6-31G* and 6-311G**basis sets. In the ^1H-NMR spectrum of $[C_8DABCO^+][(CF_3SO_2)_2N^-]$ reported in Figure 3a, one can note a triplet peak around 0.81 ppm related to the terminal methyl group **(H_a)**, while the intense signals between 1.19 and 1.27 ppm are related to methylene protons in the Octyl chain **($H_{b,c,d,e,f}$)**. The calculated ^1H chemical shifts of protons appear in the region 0.68–0.88 ppm and 0.99–1.37 ppm, respectively, which are closely matching the experimental chemical shifts. The peaks at 1.52 and 1.64 ppm indicate the presence of the methylene protons **(H_g)** proton, which are expected at 0.99 ppm and 1.47 ppm from DFT calculations. The broad singlet centered around 3.08-3.15 is attributed to DABCO hydrogens **(H_{h-i})** and in the calculated spectrum, the computed values are around 1.89 -3.74 ppm. Another triplet is observed around 3.22-3.25 ppm and is ascribed to the DABCO deshielded protons **(H_j)**; their calculated values are between 2.12 and 3.72 ppm, in good agreement with the experimental values. In the ^1H-NMR spectrum, the chemical shifts

appearing in the region 0.79–1.64 ppm indicate the alkylation reaction of the octyl chain. Considering the RMSDs values for the structures (I), (II) and (III) of 0.57, 0.57 and 0.47 ppm (see Table 1), respectively, we observed a better concordance for structure (III). For the isolated cation the value is the lowest (0.45 ppm).

In the ^{13}C-NMR spectrum (Figure 3b and Table 2), eleven signals were observed; the signals between 13.94 and 31.55 ppm can be attributed to the carbons of octyl chain. Indeed, the calculated values of carbon atoms **C_a, C_b, C_c, C_d, C_e** and **C_f** are expected between 8.46 and 27.05 ppm, while for **C_i** and **C_j** they should appear at 38.15 ppm and 44.17 ppm, respectively. Experimentally, both signals at 44.96 and 52.57 ppm are related to DABCO carbons and in theoretical calculation, the computed values are37.90 and 58.94 ppm. The signal experimentally found at 64.75 ppm is attributed to carbon (**C_h**) of methylene protons situated near to the DABCO cycle. Moreover, carbon atoms of the [$(CF_3SO_2)_2N^-$] anion appear experimentally as a downfield signal at 121.17 ppm for **C_k** and at 118.36 ppm for **C_l**. In simulated NMR spectrum, the computed values are between 115.80 and 127.84 ppm, which confirms the anionic exchange of bromide by bis(trifluoromethanesulfonyl)imide. Comparing the respective RMSDs values for the structures (I), (II) and (III) of 5.68, 5.71 and 4.74 ppm, we observed better concordance for the structure (III), as observed for the H nuclei.Here, the effect of incorporation of anion to cation is also observed in the predicted ^{13}C chemical shifts of IL which are higher, as compared with the values of cation (5.36 ppm).

Finally, in the observed ^{19}F-NMR spectrum(Figure 3c and Table 3), it is evidentthat the chemical shift for fluorine nucleiofthe –CF_3 moiety of the anion gives only a single experimental peak at -78.93 ppm while the computed chemical shifts for those three structures predict high RMSDs values, as compared with the experimental ones (35.01-50.12 ppm). Here, we use CCl_3F as reference to obtain the predicted signal of ^{19}F.In the same way, the effect of incorporation of cation to anion is also observed in the predicted ^{19}F chemical shifts of IL which are highest, as compared with the values of anion (32.72 ppm).At this time, the structure (III) evidences a clear better agreement. Such high differences could be attributed to the reference used and to the different the cation-anion interactions predicted in the three structures.

3.2. Optimizations in different media

From the above NMR studies is clear that the structure (III) (See Figure 2) is the one that best represents the [C_8DABCO$^+$][$(CF_3SO_2)_2N^-$] ionic liquid. Besides, when those three structures of IL were optimized by using the B3LYP method and the 6-31G* and 6-311G** basis sets

in gas phase and aqueous solution we observed lower energies for the structure (III). Thus, calculated total energies, dipole moments (μ) and volumes of ionic liquid in gas phase and aqueous solution, compared with the cation and anion in gas phase by using 6-311++G** basis set are summarized in **Table 1**.Whereas in **Figure S1** it is observed the optimized structure (III) together with the atoms labelling. Hence, we see that when the anion is incorporate to cation the expected volume of IL is 287.1 + 183.3 = 470.4Å^3, computed with the 6-311++G** basis set. However, the calculated volumesareslightly lower (6-311G** basis set) probably due to effect of interactions that reduce the values.Note that with the incorporation of cation the dipole moment of anion increase in remarkable form from 4.36 D in gas phase to 13.68 D and 22.53 D in (II) in both media. In (III), the dipole moment values of IL are predicted to be 13.89 and 23.29 D in gas phase and solution, respectively. Expansions of volume in the three structures are observed in solution, as a consequence of increase in the dipole moment values.In this IL, the effect of the anion on the dipole moment (μ) of the cation can be seen in **Figure S2** because it shows that the magnitude, direction and orientation of the dipole moment vector in the cation is different from the that in the IL. The direction of vector in the cation is from the C atom linked to the tertiary N atom passing through the centre towards the quaternary N atom, as it is observed in Figure S2 while the direction of the vector in the IL is perpendicular to the three rings and to the side chain. Thus, modifications in the direction, orientation and magnitude of IL are observed from the gas phase to solution. Regarding the energies values, the structure (III) present the lowest values in the two media due to basis set and,it is observed that when the total energies are corrected by Zero-point vibrational energy (ZPVE) the values decreases in all cases, as also was observed in other IL [18,19]. When the anion is incorporated to the cation the expected total uncorrected energy between cation and anion by separate is -660.2297 - 1827.6092 = -2487.0096 Hartrees, the resultant value is lower or less negative than the calculated for (III) (-2488.0891 Hartrees). Newly, the cation-anion interactions could justify such differences. B3LYP/6-311G** calculations predict the interactions presented in **Table 5**, being the S47-O49···H16 (2.261 Å) and S47-O50···H22 (2.189Å) interactions those with lower distances in gas phase while the lower distances in solution are observed in the S48-O51···H10 (2.827 Å) and C54-F55···H14 (2.654 Å) interactions. This latter interaction justifies the high ^{19}F chemical shifts predicted for the proposed structure (III) of IL because in solution the distance of C-F···Hinteraction is shorter (2.654 Å) than the other S-O···H ones (2.827 Å).

Predicted geometrical parameters for the two tertiary and quaternary N atoms of $[C_8DABCO^+][(CF_3SO_2)_2N^-]$ IL in both media and for the shorter bonds C-H lengths involved in the mentioned cation-anion interactions are compared in **Table 6** with those reported for the cation and $[C_8DABCO^+][PF_6^-]$ IL in gas phase by using the B3LYP/6-31G* method [19].In the $[C_8DABCO^+][PF_6^-]$ IL, the N-C distances in gas phase are similar to those of the cation but are different in the two media; in the $[C_8DABCO^+][(CF_3SO_2)_2N^-]$ IL there is are larger difference in the bond lengths in the two media. However, the bond angles in solution present a lower difference in the $[C_8DABCO^+][(CF_3SO_2)_2N^-]$ IL, as compared with the other one. As expected, higher variations in the geometrical parameters of tertiary N1 atoms in the two media are observed than the quaternary ones (N23) because the lone pairs of N1 are probably hydrated in solution. Evidently, the $[PF_6^-]$ anion produces higher modifications in the bond anglesrelated to N1 of $[C_8DABCO^+][PF_6^-]$ IL [19] as compared with the corresponding one for the $[(CF_3SO_2)_2N^-]$ anion of $[C_8DABCO^+][(CF_3SO_2)_2N^-]$ IL. In this latter IL, the angles related to N1 are less influenced by the anion.

3.3. Atomic charges, bond orders and molecular electrostatic potentials

Structural studies have evidenced the presence of different H bonds in the $[C_8DABCO^+][(CF_3SO_2)_2N^-]$ IL due to the acceptors and donor's groups which present different characteristics in the two media. Thus, in the gas phase the S47-O49⋯H16 and S47-O50⋯H22interactions have shorter distances while in solutionother different S48-O51⋯H10 and C54-F55⋯H14interactions with short distances are observed.To investigate such differences, three types of charges were analysed in this IL, which are Merk-Kollman (MK), Mulliken and atomic natural population analysis (NPA) charges only for the two tertiary and quaternary N atoms and the C, O and F atoms of anion in the twomedia by using the B3LYP/6-311G** method. These results are shown and compared in **Table S1** while the behaviours of these charges in the two media are presented in **Figure S3**. Here, the most important pointis that only the MK chargeson N23 show positive values in both media, as expected because they correspond to cation positively charged on quaternary N23 atoms while the Mulliken and NPA charges on N23 present negative values. Other very important results are observed in the Mulliken charges on the C53 and C54 atoms because in solution the charges on these atoms present positive values, differently from thegas phase, as shown in Figure S3b. Other important results are observed in the positive Mulliken charges on F55 and F56 in gas phase because in solution the three charges on these atoms present negative values. These differences could be attributed to different interactions where these F atoms are

involved which were not considered in Table 5, as that C54-F55···H14 interaction observed in gas phase. Note that only the Mulliken charges on O49 and O50 show positive values in gas phase but negative ones in solution, as the other ones, justifying this way, the enlargement of the interactions in solution where these atoms are involved.

The molecular electrostatic potentials (MEP) and bond orders (BO), expressed as Wiberg indexes of IL were also studied because they are essential factors to analyse the different reaction sites and the different strength of bonds. These parameters for the $[C_8DABCO^+][(CF_3SO_2)_2N^-]$ IL in both media are presented in **Table S2**. Thus, the exhaustive analyses of MEP values on all considered atoms show practically few changes of values in solution and the typical MEP tendency taking into account the different electronegativity of atoms (F > O > N > C). Note that the F (F60) and O atoms (O49, O50 and O51) involved in the H bonds present lower MEP values. Obviously, the H atoms present the less negative MEP values, as expected because they are the most labile atoms. When the mapped surfaces of $[C_8DABCO^+][(CF_3SO_2)_2N^-]$ IL in both media are shown in **Figure S4** we can see the different nucleophilic and electrophilic sites of reaction. Thus, the three fused rings show blue colours, as expected because the quaternary N23 is positively charged and are electrophilic sites while the strong red colours are observed on the O, N and F atoms of anion due to the lone pairs of these atoms, thus, the reaction sites are nucleophilic.The MEP surfacesof IL in both media change from 0.069 a.u. in gas phase to 0.085 a.u. in solution.

Evaluating the bond orders totals by atom, expressed as Wiberg indexes of IL in the twomedia by using the same level of theory from Table S2, it is observed that the O49, O51 and F60 present slight differences in solution due to the formation of H bonds. When Wiberg bond index matrix in the NAO basis are calculated from NBO calculations it is observed that S47-O50···H22 interaction in gas phase has a BO of 0.0124 higher than the predicted 0.0075 for the S47-O49···H16 interaction while in solution the S48-O51···H10 interaction presents a bond order of 0.0022 similar to the value predicted for the C54-F55···H14 interaction of 0.0023. These results show that the interactions are different in the two media, as was previously mentioned.

3.4. NBO and AIM studies

The stability of the $[C_8DABCO^+][(CF_3SO_2)_2N^-]$ IL was studied by using two different procedures because the presence of two tertiary and quaternary N atoms produce different interactions in gas phase and aqueous solution. One of them is by using the NBO program in order to calculate the acceptors-donors interactions energies with the Second Order Perturbation Theory Analysis of Fock Matrix in NBO Basis [27] while the other one is by

using the Bader's theory of atoms in molecules with the AIM 2000 program [28,29]. In the first case, the calculated acceptors-donors interactions energies (E2) by using NBO calculations [27] are summarized in **Table S3**. Only two types of interactions are predicted for the IL in both media. One of them consists of the$n \rightarrow \sigma^*$ interactions from lone pairs of N, O and F atoms of the anion to different antibonding S-O, S-C, N-S and C-F orbitals, while the other ones are the $\sigma^* \rightarrow \sigma^*$ interactions. These latter transitions have low energy values and occur from antibonding N-S and S-Oorbitals to antibonding N-S, C-F or S-O orbitals, as observed in Table S3. The contribution of those two types of transitions to the total energy is of 1906.92 kJ/molin gas phase and of 2017.23 kJ/mol in solution. Hence,the proximities in the values suggest that the IL presents practically the same stability in both media.

In the other study of intramolecular interactions by using the Bader's theory, the topological properties of IL (electron density, $\rho(r)$, the Laplacian values, $\nabla^2\rho(r)$, the eigenvalues $(\lambda 1, \lambda 2, \lambda 3)$ of the Hessian matrix and, the $|\lambda 1|/\lambda 3$ ratio) were computed with the AIM 2000 program in the bond critical points (BCPs),ring critical points (RCPs) andcage critical points (CCP) [28,29].**Table S4** shows the different and similar intramolecular interactions predicted for the IL in the two media by using the B3LYP/6-311G** method. In gas phase there are nine predicted BCPs (7 C-O···H, C-F···H and C-F···O), eleven new RCPNs in addition to the three RCPs of rings and, four CCPs, while in solution only eight BCPs (five C-O···H, C-F···H, C-F···O and C-H···H), nine RCPNs, three RCPs and three CCPs are predicted. The ring critical points formed as a consequence of new H bonds interactions are named RCPNs. All interactions for IL in both media are shown and clearly indicated in **Figure S5**. The characteristics of intramolecular H bonds interactions are different in the two media; the shortest two interactions in both media are specified in **Table S5** by using bold letters (See distances in Table S5). Note that the C53-F60···H29 interaction is predicted in gas phase while, on the contrary,only the C53-F55···H14 interaction is expected in solution. Figure S5 shows that in gas phase only the F55 and F60 atoms are involved in intramolecular interactions while in solution only the F55 is taking part in.These studies show that the IL form different intramolecular H bonds in the two media but in both cases only two of them present short distances. Thus, the two NBO and AIM studies reveal that IL has practically the same stability in the two media.

3.5. Frontier Orbitals studies

NBO calculations evidenced approximate energy values of $[C_8DABCO^+][(CF_3SO_2)_2N^-]$ IL in both media (1906.92/2017.23 kJ/mol) whilethe AIM studies also predict similar stabilities in

these media due to eight/nine new intramolecular H bonds interactions; however, reactivities, stability kinetic and behaviours of IL in the two media have not yet been investigated. Therefore,to predict the reactivity and behaviours in the two media,the frontier orbitalsshould be computed and from their differences the gap values are obtained. After that, with these parameters theglobal hardness (η), global softness (S) and global electrophilicity index (ω) descriptors can be calculated.Accordingly, **Table S6** shows calculated HOMO and LUMO orbitals, energy band gap, global hardness (η), global softness (S) and global electrophilicity index (ω) for the $[C_8DABCO^+][(CF_3SO_2)_2N^-]$ ionic liquid in gas phase and aqueous solution by using the B3LYP/6-311G** method. The parameters for cation and anion in gas phase by using the B3LYP/6-311++G** method, respectively can be also observed in the table while the gap value in gas phase for the cation using the 6-31G* basis set is 7.1512 eV [18,39]. Regarding Table S6, we observed that the gap values of $[C_8DABCO^+]$ cation and $[(CF_3SO_2)_2N^-]$ anion are different between them (6.4818/7.2600 eV) [18,39] but the ionic crystalpresents lower values in both media, as compared tothe anion.Thus, the incorporation of anion to cation generate lower gap value in solution but higher in gas phase. Hence, the $[C_8DABCO^+][(CF_3SO_2)_2N^-]$ IL is more reactive in solution than the two separated species. Comparing the gap value of IL in solution (5.7389 eV) with the one reported for $[C_8DABCO^+][Br^-]$ IL (5.0558 eV), it is clear that $[C_8DABCO^+][(CF_3SO_2)_2N^-]$ is less reactive [18]. As a consequence, the effect of $[Br^-]$ on $[C_8DABCO^+]$ is higher than thatobserved for $[(CF_3SO_2)_2N^-]$ on the cation of IL, specifically in solution. However, the $[PF_6^-]$ anion increases the gap values of $[C_8DABCO^+][PF_6^-]$ to 7.4368 eV in gas phase and 7.4668 eV in solution [19].When the characteristics and forms of frontier orbitals of IL in both media are carefully analysed from **Figure S6,** we observed that orbitals belonging to the atoms of cage-like DABCO structure participateto LUMO in both media,while the anion participateto HOMO in both media, even though in the gas phase also the N1 orbital and some C orbitals contribute to HOMO. Probably, this observation justifies the lower reactivity of IL, the lower total energy (1906.92 kJ/mol) and the eight new intramolecular interactions predicted by AIM analyses in this media. Thus, the participation of orbitals belonging to the atoms of cage-like DABCO structure and of anion in both HOMO and LUMO suggest thatcation and anion are engaged in the different interactions predicted by NBO and AIM calculations. Consequently, the DABCO structureplay very important role in the properties of IL in the two media, as also was observed in $[C_8DABCO^+][PF_6^-]$ IL [19]. The evaluation of descriptors suggests that the higher reactivity of IL in solution could be associated to its higher global electrophilicity index (ω).Note that the effect of anion on IL in gas phase is the decreasing of

global electrophilicity index (ω) of cation from 7.7572 eV to 2.0720 eV or the increase of gap value from 6.4818 eV to 6.7756 eV in the IL.

3.6. Vibrational analyses

The structure of $[C_8DABCO^+][(CF_3SO_2)_2N^-]$ IL was optimized by using the B3LYP/6-311G** method with*C_1* symmetry and with the two CF_3 groups of anion in*Trans* position. Due to the 60 atoms present in IL in total 174 normal vibration modes are expected. All vibration modes present activity in both infrared and Raman spectra. In **Figures 4** and **5** the experimental FT-IR and FT-Raman spectra of IL in the solid phase are compared with the corresponding spectra predicted for IL and its cation and anion in the gas phase at different levels of theory. **Figure S7**shows comparisons of experimental FT-IR spectrum of IL with the corresponding predicted for IL in gas phase and aqueous solution by using the B3LYP/6-311G** level of theory.Note that the IR spectra of IL in both media are practically the same and only slight variations in the intensities of bands in the region 2000-1000 cm^{-1} are observed.On the other hand, Figures 4 and 5 show better correlations in the Raman spectra, in particular because the predicted Raman spectra were corrected from activities to intensities [35]. Figure 4 shows that for the IL and anion the bands between 2000 and 1000 cm^{-1} are predicted with higher intensities, as compared with the experimental one. Hence,the effect of the cation justifies the lower intensities observed in the experimental IR spectrum.The harmonic force fields for the IL in both media were calculated with the scaled quantum mechanical force field (SQMFF) methodology and the Molvib program [32-34]. For this IL, the normal internal coordinates of cation (129 vibration modes) and anion (39 vibration modes) previously reported were used [18,39] while six new internal coordinates due to the two S-O⋯H interactions were addeduntil completing the 174 vibrations expected. Here, transferable scaling factors were used for IL [33]. **Table 7** shows assignments for IL, cation and anion together with experimental and calculated wavenumbers by using the hybrid B3LYP method and different levels of theory [18,39]. Here, we reported the complete vibrational assignments for the 174 vibration modes of IL. We observed from Table 7 that cation shifts the bands of anion toward higher wavenumbers in the IL, as a consequence of interactions due to H bonds. Below, some main assignments are discussed by regions.

3.6.1. Assignments C-H groups.

3.6.1.1. 4000-2000 cm^{-1} region. In this region, only the antisymmetric and symmetric stretching modes of CH_2 and CH_3 groups of cation are expected [18,19,39]. Here, the anion shows a clear effect on cation because the assignments predict for the IL with the B3LYP/6-

311G** level of theory are different from those predicted for the cation by using the B3LYP/6-31G* method [18,19]. In part, the difference can be attributed to the different methods used and in part to the cation-anion interactions evidenced by NBO and AIM studies. Then, the IR bands and shoulders observed in this region are assigned to those vibration modes, as specified in Table 7. The intense Raman band observed at 2966 cm^{-1} are assigned to symmetric CH_2 stretching modes,as expectedwhile the strong band at 2901 cm^{-1} can be assigned to symmetric CH_3 stretching mode. In the $[C_8DABCO^+][PF_6^-]$ IL [19], the symmetric CH_2 stretching modes are assigned to the band at 2974 cm^{-1}.

3.6.1.2. 2000-1000 cm^{-1} region. In this region, the vibration modes corresponding to CH_3 and CH_2 deformation, CH_2 wagging, CH_3 and CH_2 rocking modes are expected [18,19,39]. However, the SQM calculations predict at 1966 cm^{-1} the wag CH_2(C3) mode and at 1507 cm^{-1} a torsion mode (τO49-H16) related to S47-O49···H16-C6 interaction and to adeformation CH_2 mode due to the same interaction (δCH_2(C6)). The assignment of waging mode in that unexpected frequency is justified by the other S48-O51···H10-C3 interaction where the C3 atom is involved. The IR and Raman bands observed in the spectra of IL between 1934 and 1133 cm^{-1} are assigned to CH_3 and CH_2 deformation, CH_2 wagging, CH_3 and CH_2 rocking modes of cation, as predicted by SQM calculations while the antisymmetric and symmetric stretching modes of SO_2 and CF_3 groups are predicted from 1244 to 1028 cm^{-1}. In some cases, the antisymmetric SO_2 and CF_3 stretching modes are predicted coupled between them at 1197 and 1166 cm^{-1}. Thus, the intense IR and Raman bands at 1243, 1180, 1133, 1058 and 1052 cm^{-1} are clearly assigned to those vibration modes, as predicted by SQM calculations. The symmetric stretching modes of two CF_3 groups are predicted in the anion at 1150 and 732 cm^{-1} while in the IL at 751 cm^{-1} not as a pure mode but coupled with a deformation mode at 737 cm^{-1}. Hence, the very strong Raman band at 739 cm^{-1} is assigned to those vibration modes. The IR and Raman bands between 1052/1058 and 1015 cm^{-1} are assigned to C-C and C-N stretching modes.

3.6.1.3. 1000-10 cm^{-1} region. Here, the CH_3 and CH_2 twisting and C-C and C-N stretching and CCN, CCC skeletal modes of cation are expected together with vibration modes of anion [18,19,39]. The CH_2 twisting modes are predicted in the cation between 936 and 662 cm^{-1} while in the IL between 935 and 655 cm^{-1}. Evidently, these modes are poorly influenced by the anion but they appear strongly coupled as a consequence of cation-anion interactions. Here, it is observed that the SO_2 wagging mode related to the S47-O49···H16-C6 interaction is predicted at 280 cm^{-1} while for the other group is predict at 581 cm^{-1}; however, in the anion

both modes are predicted at 616 and 568 cm^{-1}. Hence, we can easily see the influence of cation on anion. Another thing, the deformation, rocking and twisting modes of SO_2groups and rocking and twisting modes of CF_3 groups are marginally influenced by the cation-anion interactions, as observed in Table 7.

3.7. Scaled force constants

Scaled force constants are interesting parameters that show how the interactions present in a compound can affectits properties and, also bond lengths and angles, vibration modes and force constants, such as those cation-anion interactionspredicted in this IL. For these reasons, for $[C_8DABCO^+][(CF_3SO_2)_2N^-]$ IL in both media those factors were computed from the previously obtained harmonic force fields with the SQMFF methodology and the Molvib program [32-34]. Hence, in **Table 8** are summarized the scaled internal force constants for the $[C_8DABCO^+][(CF_3SO_2)_2N^-]$ ionic liquid in both media and for its $[C_8DABCO^+]$cation and $[(CF_3SO_2)_2N^-]$ anion in gas phase by using the hybrid B3LYP method and different basis sets [18,19,39].Comparing first the force constants for IL in both media, we observed important and significant variations in the *f(νN-C)*, *f(νSO₂)*, *f(δSO₂)* and *f(δCH₂)*force constants when the medium change from the gas phase to aqueous solution.Obviously, these discrepancies are associated to the different interactions predicted for IL mainly by NBO and AIM calculations. Thus, from Table 5 two interactions in each medium were predicted with short distances, which are, S47-O49···H16-C6 and S47-O50···H22-C20 in gas phase while other different S48-O51···H10-C3 and C54-F55···H14-C5 in solution. Higher distances are observed in the gas phase because the molecules have greater freedom of movement due to that the forces of crystalline packing were not considered. Hence, the main SO_2 groups and some F and C atoms of CF_3 and CH_2 groups are involved in these cation-anion interactions and, as a consequence, the force constants related change with the medium. Then, when the force constants of cation are compared with the two ILs, only the *f(νN-C)* and *f(δCH₂)* force constants show changes with the medium, being more evident in this IL, as compared to $[C_8DABCO^+][Br^-]$ [18]. If now the force constants for IL are compared with the corresponding anion we observed that the *f(νSO₂)* and *f(δSO₂)* force constants of IL show strong changes in solution which are attributed to cation-anion interactions. The different values observed in the main force constants of IL in both media supports the different cation-anion interactions predicted for IL in the two media.

3.8. Thermal analysis

One of the most important properties of ionic liquidsistheir thermal behaviour and the temperature range of application. These properties depend on the ionic structure of anions and cations. To obtain information on the thermal stability and degradation of $[C_8DABCO^+][(CF_3SO_2)_2N^-]$, the thermal properties were investigated in the temperature range [25°C /700°C] using thermogravimetric analysis (TGA) and in the interval [-80 / 200 °C] by differential scanning calorimetry (DSC) on heating the sample. As shown in **Figure 6**, $[C_8DABCO^+][(CF_3SO_2)_2N^-]$shows a small endothermic peak at -51 °C corresponding to the glass transition (T_g). The exothermic peak at -13°C is associated with the so-called cold crystallization. Finally, a clear endothermic peak at 27°C corresponds to the melting process (T_m).As the melting point is lower than 100°C, $[C_8DABCO^+][(CF_3SO_2)_2N^-]$ can be classified as an ionic liquid. Regarding the TGA results, the thermal decomposition of $[C_8DABCO^+][(CF_3SO_2)_2N^-]$ occurs in the temperature range [350°C /470°C], and reaches a mass loss of 100% at 470 °C. The high decomposition temperature of the sample suggests that that it could be adequate for applications as electrolyte for electrochemical devices.

4. Conclusions

In this investigation, the $[C_8DABCO^+][(CF_3SO_2)_2N^-]$ IL was prepared and its structure characterized and confirmed by using ^1H, ^{13}C and ^{19}F–NMR, IR and Raman spectroscopies. In addition, its thermal stability and decomposition process were studiedby using TGA andDSC analyses. Theoretically, three different structures (I), (II) and (III) were proposed for this IL where the CF_3 groups of anion present *Cis* or *Trans* positions. Comparisons among the experimental ^1H, ^{13}C and ^{19}F–NMR, IR and Raman spectra with the corresponding predicted for those structures have evidenced better correlations with the structure (III) optimized by using the hybrid B3LYP/6-311G** method in gas phase and aqueous solution. Hence, structural, electronic and topological properties were predicted for this structure of IL in gas phase and aqueous solution. Hybrid B3LYP/6-311G** calculations predict two S47-O49⋯H16-C6 and S47-O50⋯H22-C20 interactions in gas phase and other two S48-O51⋯H10-C3 and C54-F55⋯H14-C5 in solution where the latter interaction could justifythe high predicted ^{19}F chemical shifts for the proposed structure (III) of IL because in solution the distance of C-F⋯Hinteraction is shorter (2.654 Å) than the other S-O⋯H ones (2.827 Å). The studies of charges show that only the MK charges on quaternary N23 atoms in both media are positively charged because they belong to cation while the positive Mulliken charges on O49 and O50 in gas phase become negative in solution and justify those two interactions in this medium. The mapped MEP surfaces support the electrophilic sites on

positive charges of quaternary N23 while the nucleophilic sites are observed on the O, N and F atoms of anion.The NBO and AIM calculations show that the characteristics of cation-anion interactions predicted for the IL in gas phase are different from those predicted in solution, as suggested by the different values observed in the *f(νN-C)*, *f(νSO$_2$)*, *f(δSO$_2$)* and *f(δCH$_2$)* force constants in both media. The gap values suggest that [C_8DABCO$^+$][$(CF_3SO_2)_2N^-$] is less reactive than [C_8DABCO$^+$][Br^-] IL while the characteristics of frontier orbitals justify the cation-anion interactions and support the important role of DABCO in the properties of IL in the two media. The complete assignments of 174 vibration modes expected for IL are reported together with the scaled force constants.

Declaration of Competing Interest

The authors declare that they have no known competing financial interests or personal relationships that could have appeared to influence the work reported in this paper.

CRediT authorship contribution statement

Boumediene Haddad: Writing – original draft, Conceptualization, Data curation, Writing – review & editing, Supervision. Silvia Antonia Brandán: Validation, Visualization, Writing– original draft, Writing – review & editing. BekhaledFetouhi: Methodology, Data curation. MostefaBoumediene: Conceptualization, Data curation. Annalisa Paolone: Conceptualization, Data curation. Didier Villemin: Conceptualization, Project administration. Mustapha Rahmouni: Conceptualization, Data curation. Serge Bresson: Methodology, Resources.

Acknowledgements

This work was supported with grants from financial support by The Ministry of Higher Education and Scientific Research (MESRS) of Algeria in PRFU project code: B00L01UN200120180002 and, from CIUNT Project Nº 26/D608(Consejo de Investigaciones, Universidad Nacional de Tucumán). The authors would like to thank Prof. Tom Sundius for his permission to use MOLVIB.

Supporting Information Available: Tables S1-S6 and Figures S1-S7.

References

[1] Z. Lei, B. Chen, Y.-M. Koo, D.R. MacFarlane, Introduction: Ionic liquids, Chem Rev. 117 (2017) 6633–6635.
[2]B. Haddad, S.A. Brandán, M.A. Assenine, A. Paolone, D. Villemin, S. Bresson, Bidentate cation-anion coordination in the ionic liquid 1-ethyl-3-methylimidazolium hexafluorophosphate supported by vibrational spectra and NBO, aim and SQMFF calculations, J. Mol. Struct. 1212 (2020) 128104.
[3] M.H. Mruthunjayappa, N.S. Kotrappanavar, D. Mondal, New prospects on solvothermal carbonisation assisted by organic solvents, ionic liquids and eutectic mixtures – a critical review, PROG MATER SCI. 126 (2022) 100932.
[4]I. Baskin, A. Epshtein, Y. Ein-Eli, Benchmarking machine learning methods for modeling physical properties of ionic liquids, J Mol Liq. 351 (2022) 118616.
[5] S.S. de Jesus, R. MacielFilho, Are ionic liquids eco-friendly?,Renewable Sustainable Energy Rev. 157 (2022) 112039.
[6] K.U. Sivakami, S. Vaideeswaran, A.R. Venis, J.K.A. Juliet Helina, M. Balaganesh, Impregnation, silver activating capability and biological applications of ionic liquids, *Mater. Lett*: X. 13 (2022) 100134.
[7] A. Damokhi, S. Yousefinejad, R. Yarmohammadi, S. Jafari, Ionic liquids in biological monitoring for exposure assessments, J Mol Liq. 344 (2021) 117732.
[8]Z.S. Qureshi, K.M. Deshmukh, B.M. Bhanage, Applications of ionic liquids in organic synthesis and catalysis, CleanTechnolEnvir. 16 (2013) 1487–1513.
[9]B. Haddad, D. Villemin, E.-habibBelarbi, Synthesis of palladium-bidentate complex and its application in Sonogashira and Suzuki coupling reactions, Chem Pap. 68 (2014).
[10]B. Haddad, D. Mokhtar, M. Goussem, E.-habibBelarbi, D. Villemin, S. Bresson, et al., Influence of methyl and propyl groups on the vibrational spectra of two imidazolium ionic liquids and their non-ionic precursors, J. Mol. Struct. 1134 (2017) 582–590.
[11] B. Haddad, J. Kiefer, H. Brahim, E.-habibBelarbi, D. Villemin, S. Bresson, et al., Effects of C(2) methylation on thermal behavior and interionic interactions in imidazolium-based ionic liquids with highly symmetric anions, ApplSci-Basel. 8 (2018) 1043.
[12] S.K. Panja, B. Haddad, J. Kiefer, Clusters of the ionic liquid 1-hydroxyethyl-3-methylimidazolium picrate: From theoretical prediction in the gas phase to experimental evidence in the Solid State, ChemPhysChem. 19 (2018) 3061–3068.
[13] S.K. Panja, B. Haddad, M. Debdab, J. Kiefer, Y. Chaker, S. Bresson, et al., Cluster formation through hydrogen bond bridges across chloride anions in a hydroxyl-functionalized ionic liquid, ChemPhysChem. 20 (2019) 936–940.
[14] B. Haddad, A. Paolone, D. Villemin, J.-F. Lohier, M. Drai, S. Bresson, et al., Para-xylyl bis-1-methylimidazolium bis(trifluoromethanesulfonyl)imide: Synthesis, crystal structure, thermal stability, Vibrational Studies, J Mol Liq. 260 (2018) 391–402.
[15]K. Low, S.Y. Tan, E.I. Izgorodina, An ab initio study of the structure and energetics of hydrogen bonding in Ionic liquids, Front Chem. 7 (2019). https://doi.org/10.3389/fchem.2019.00208[16] M. Ishtiaq, M.A. Khan, S. Ahmed, S. Ali, M. al-Rashida, S. Iftikhar, et al., Probing new DABCO-F based ionic liquids as catalyst in organic synthesis, J. Mol. Struct. 1268 (2022) 133638.
[17]N. Safari, F. Shirini, H. Tajik, Preparation and characterization of a novel Dabco based tetra cationic ionic liquid as a reusable catalyst for the multi-component synthesis of 2H-indazolo[2,1-B]phthalazine-Trione and [1,2,4]triazoloquinazolinone derivatives under solvent-free condition, J. Mol. Struct. 1201 (2020) 127143.
[18] B. Fetouhi, B. Haddad, S.A. Brandán, A. Paolone, D. Villemin, M. Boumediene, et al., Synthesis, molecular structure, and properties of DABCO bromide based Ionic liquid combining spectroscopic studies with DFT Calculations, J. Mol. Struct. 1233 (2021) 130102.
[19] B. Haddad, S.A. Brandán, B. Fetouhi, M. Boumediene, A. Paolone, D. Villemin, et al., Synthesis, NMR, vibrational spectroscopy, thermal and DFT studies of new DABCO hexafluorophosphate based Ionic Liquid, J. Mol. Struct. 1258 (2022) 132682.
[20] A.D. Becke, Density-functional exchange-energy approximation with correct asymptotic behavior, Phys. Rev. A38 (1988) 3098-3100.

[21] C. Lee, W. Yang, R.G. Parr, Development of the Colle-Salvetti correlation-energy formula into a functional of the electron density. Phys. Rev. B37 (1988) 785-789.
[22] A.B. Nielsen, A.J. Holder, Gauss View 5.0, User's Reference, GAUSSIAN Inc., Pittsburgh, PA, 2008.
[23] M.J. Frisch et al, Gaussian, Inc., Wallingford CT, 2009.
[24] S. Miertus, E. Scrocco, J. Tomasi, Electrostatic interaction of a solute with a continuum. Chem. Phys. 55 (1981) 117–129.
[25] J. Tomasi, J. Persico, Molecular Interactions in Solution: An Overview of Methods Based on Continous Distributions of the Solvent, Chem. Rev. 94 (1994) 2027-2094.
[26] A.V. Marenich, C.J. Cramer, D.G. Truhlar, Universal solvation model based on solute electron density and a continuum model of the solvent defined by the bulk dielectric constant and atomic surface tensions, J. Phys. Chem.B113 (2009) 6378-6396.
[27]E.D. Glendening, J.K. Badenhoop, A. D. Reed, J. E. Carpenter, F. Weinhold, NBO 3.1; Theoretical Chemistry Institute, University of Wisconsin; Madison, WI, 1996.
[28] R.F.W. Bader, Atoms in Molecules, A Quantum Theory, Oxford University Press, Oxford, 1990, ISBN: 0198558651.
[29] F. Biegler-Köning, J. Schönbohm, D. Bayles. AIM 2000; A Program to Analyze and Visualize Atoms in Molecules, J. Comput. Chem. 22 (2001) 545.
[30] B.H. Besler, K.M. Merz Jr, P.A. Kollman, Atomic charges derived from semiempirical methods, J. Comp. Chem. 11 (1990) 431-439.
[31] P. Ugliengo, MOLDRAW Program, University of Torino, Dipartimento Chimica IFM, Torino, Italy, 1998.
[32] P. Pulay, G. Fogarasi, G. Pongor, J.E. Boggs, A. Vargha, Combination of theoretical ab initio and experimental information to obtain reliable harmonic force constants. Scaled quantum mechanical (QM) force fields for glyoxal, acrolein, butadiene, formaldehyde, and ethylene. J. Am. Chem. Soc., 105 (1983) 7073.
[33] G. Rauhut, P. Pulay, Transferable Scaling Factors for Density Functional Derived Vibrational Force Fields. J. Phys. Chem. 99 (1995) 3093-3100, https://doi.org/10.1021/j100010a019
[34] T. Sundius, Scaling of ab-initio force fields by MOLVIB. Vib. Spectrosc. 29 (2002) 89-95.
[35]G. Keresztury, S. Holly, G. Besenyei, J. Varga, A.Y. Wang, J.R. Durig. Vibrational spectra of monothiocarbamates-II. IR and Raman spectra, vibrational assignment, conformational analysis and ab initiocalculations of S-methyl-N,N-dimethylthiocarbamateSpectrochim. Acta, 49A (1993) 2007-2026.
[36] R. Ditchfield, Self-consistent perturbation theory of diamagnetism. I. A gage-invariant LCAO (linear combination of atomic orbitals) method for NMR chemical shifts, Mol Phys. 27 (1974) 714–722.
[37] R. G. Pearson, Absolute electronegativity and hardness correlated with molecular orbital theory, Proc. Natl. Acad. Sci., USA. 83 (1986) 8440-8441.
[38] R. G. Parr, L.V. Szentpaly, S. Liu, Electrophilicity Index, J. Am. Chem. Soc., 121 (1999) 1922-1924.
[39]M.A. Assenine, B. Haddad, A. Paolone, S.A. Brandán, D. Villemin, M. Boumediene, M. Rahmouni, S. Bresson, Synthesis, thermal properties, vibrational spectra and computational studies of Trioctylmethylammoniumbis (trifluoromethylsulfonyl) imide ionic liquid, J. Mol. Struct. 1232 (2021) 130085.

Figure Caption

Scheme 1.General synthesis of $[C_8DABCO^+][(CF_3SO_2)_2N^-]$.

Figure 1. Optimized theoretical structures(I) and (II) of $[C_8DABCO^+][(CF_3SO_2)_2N^-]$IL by using the hybrid B3LYP/6-31G* methodtogetherwithintramolecular H-bonds represented with dashed lines.

Figure 2. Optimized theoretical structure (III) of $[C_8DABCO^+][(CF_3SO_2)_2N^-]$IL by using the hybrid B3LYP/6-311G** methodtogether withintramolecular H-bonds represented with dashed lines.

Figure 3. a) Hydrogen atom labeling and ^{1}H-NMR spectrum (upper panel), b) carbon atom labeling and ^{13}C-NMR spectrum (intermediate panel) and c) ^{19}F-NMR spectrum (lower panel) of ($[C_8DABCO^+][(CF_3SO_2)_2N^-]$).

Figure 4. Experimental FT-IR spectrum of ionic liquid in the solid phase compared with the corresponding predicted for IL and its cation and anion in the gas phase at different levels of theory.

Figure 5. Experimental FT-Raman spectrum of ionic liquid in the solid phase compared with the corresponding predicted for IL and its cation and anion in the gas phase at different levels of theory.

Figure 6: TGA and DSC curves of ($[C_8DABCO^+][(CF_3SO_2)_2N^-]$) Ionic Liquid, both measured on heating.

HIGHLIGHTS

- The $[C_8DABCO^+][(CF_3SO_2)_2N^-]$ IL was prepared by an alkylation reaction.
- IL was characterized by ^1H-, ^{13}C-, and ^{19}F-NMR, IR and Raman spectroscopies.
- Two different cation-anion interactions were predicted for IL in gas phase and in aqueous solution.
- NBO and AIM calculations reveal the nature of cation-anion interactions.
- Frontier orbitals support the important role of DABCO in the properties of IL.

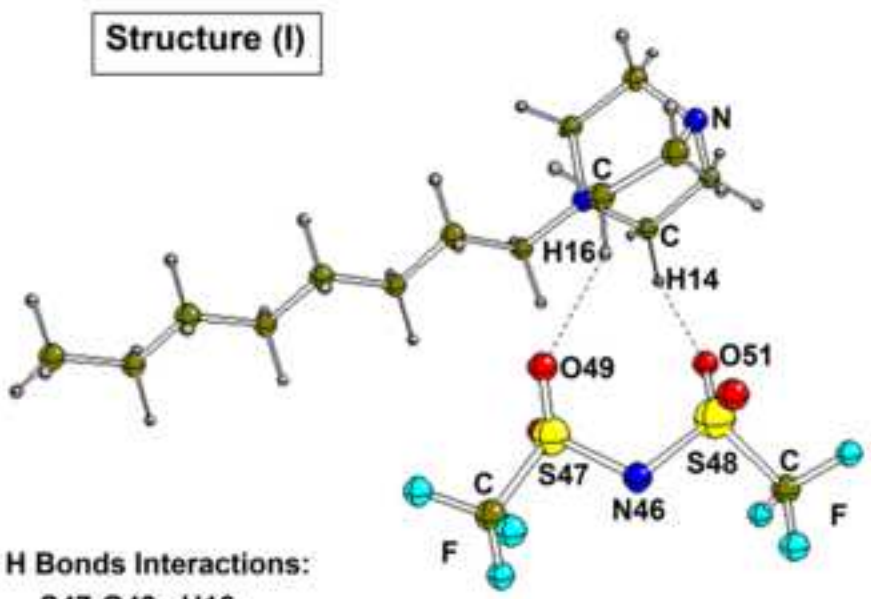

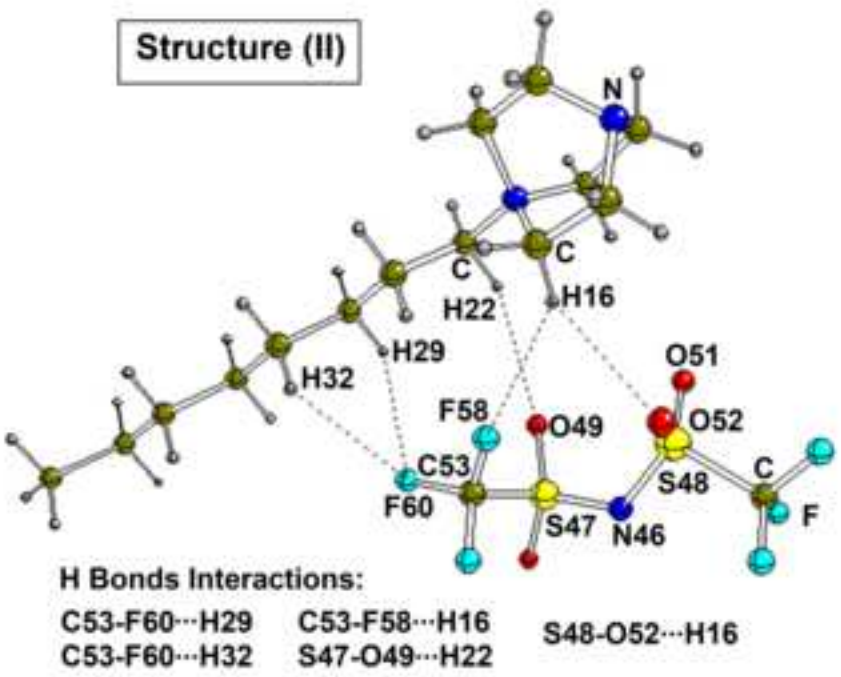

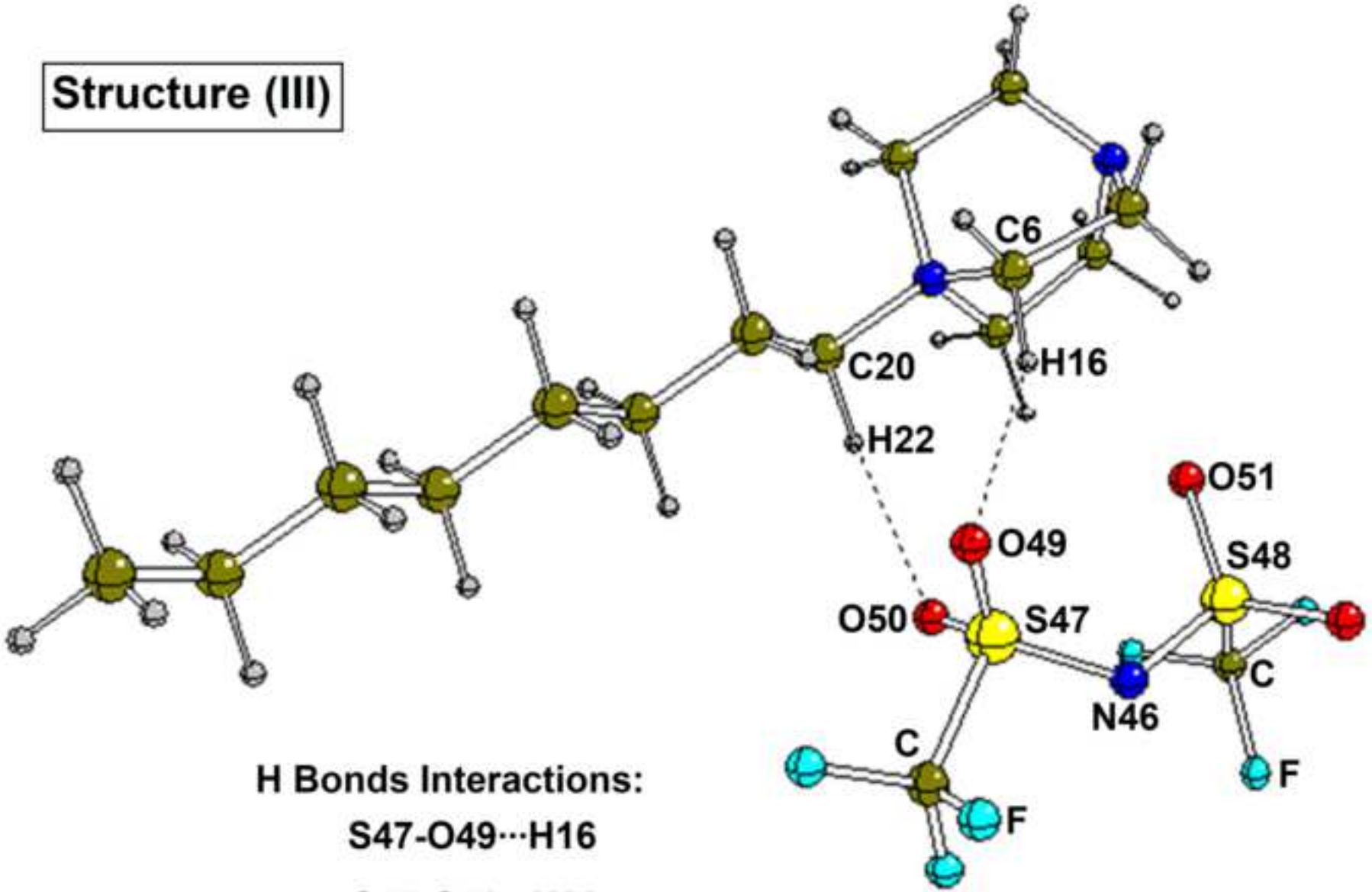

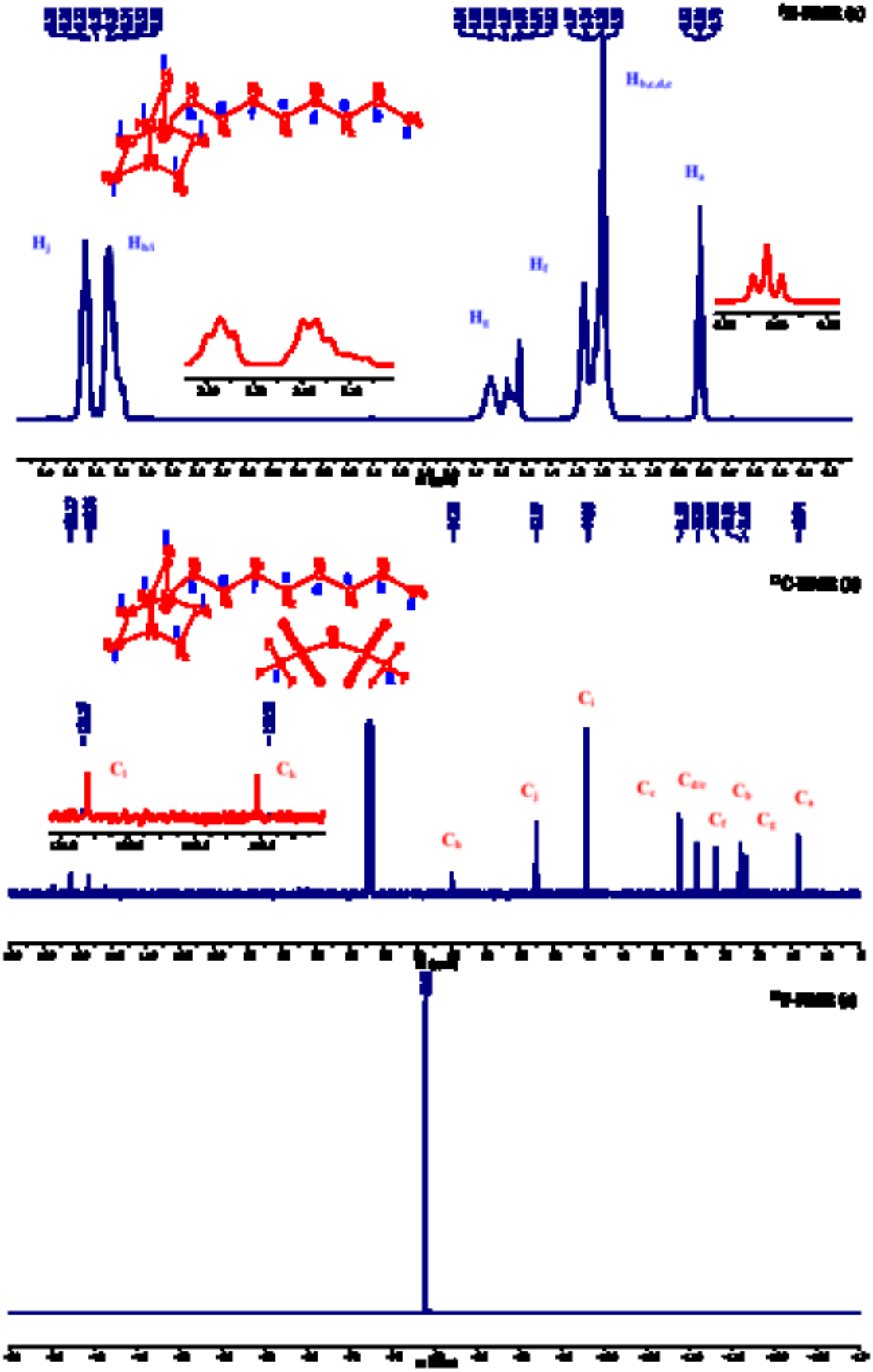

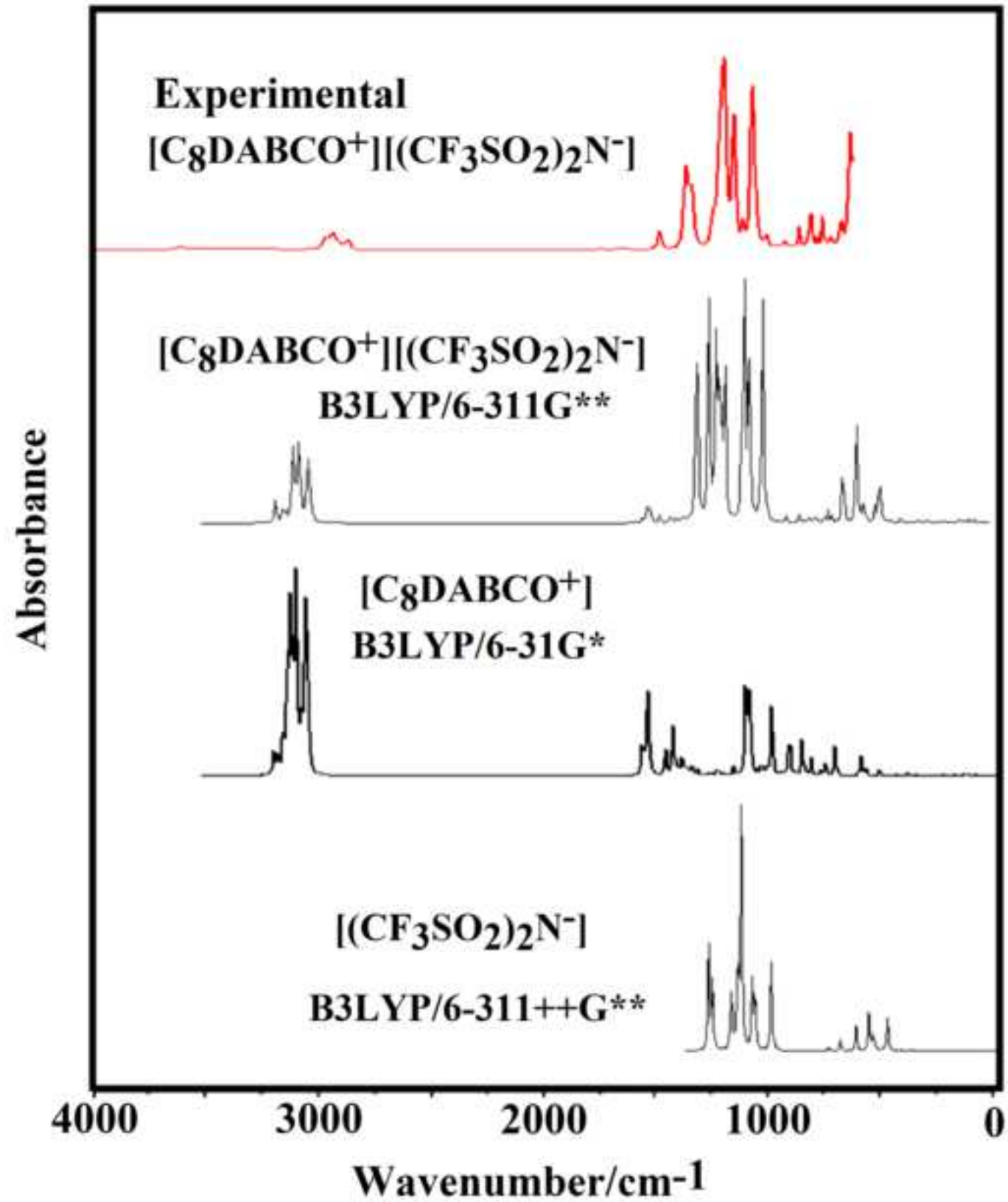

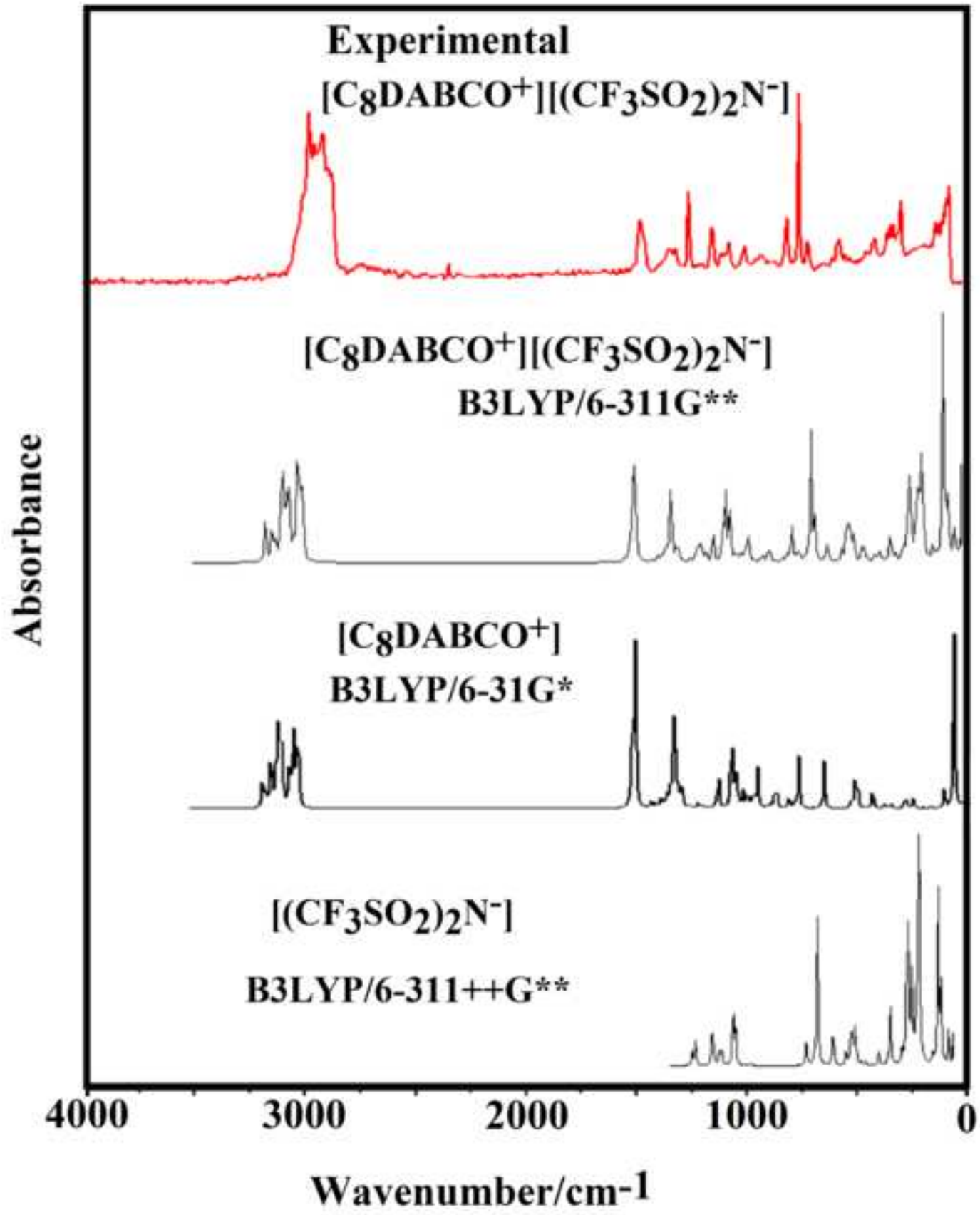

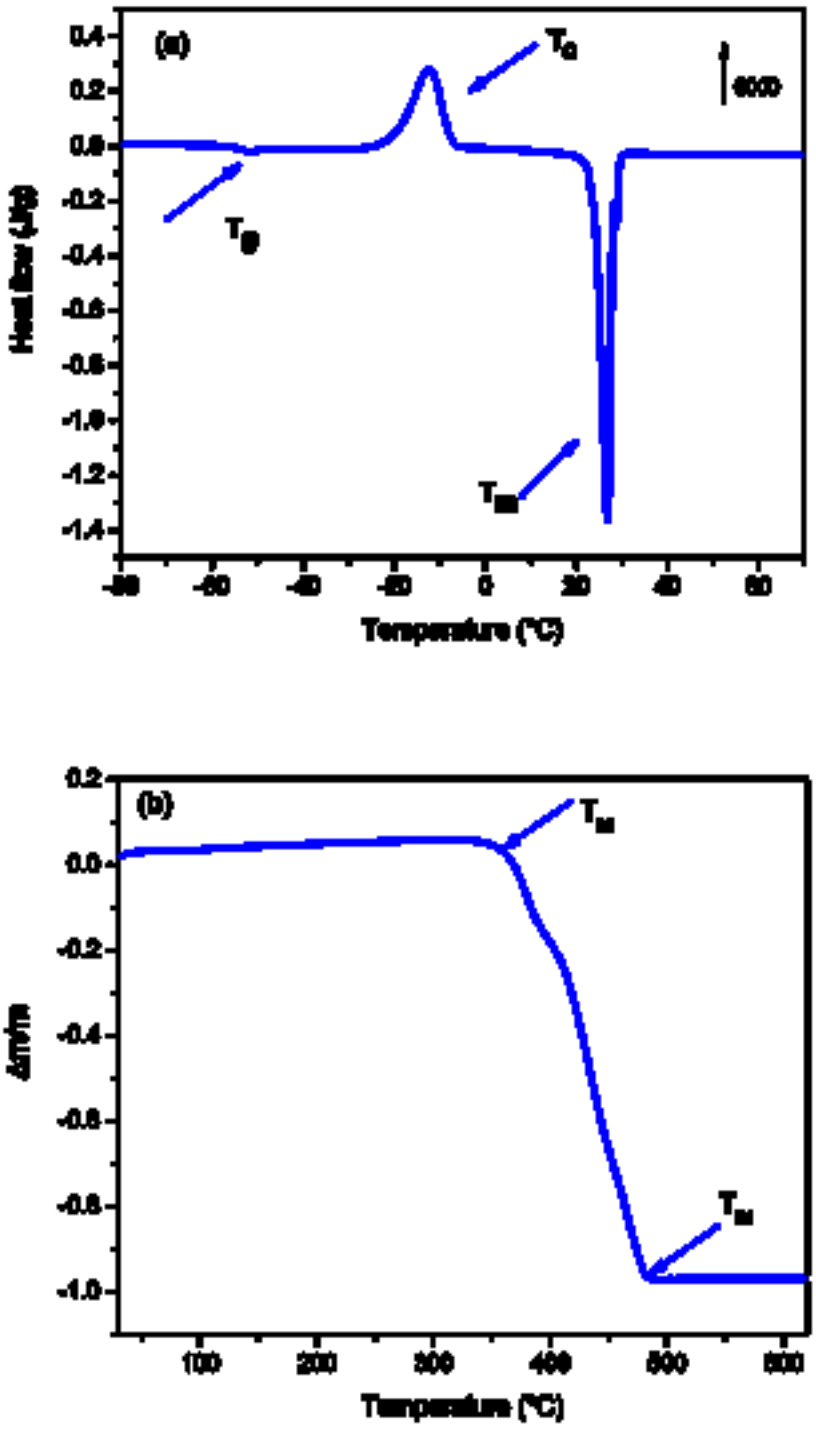

Scheme 1

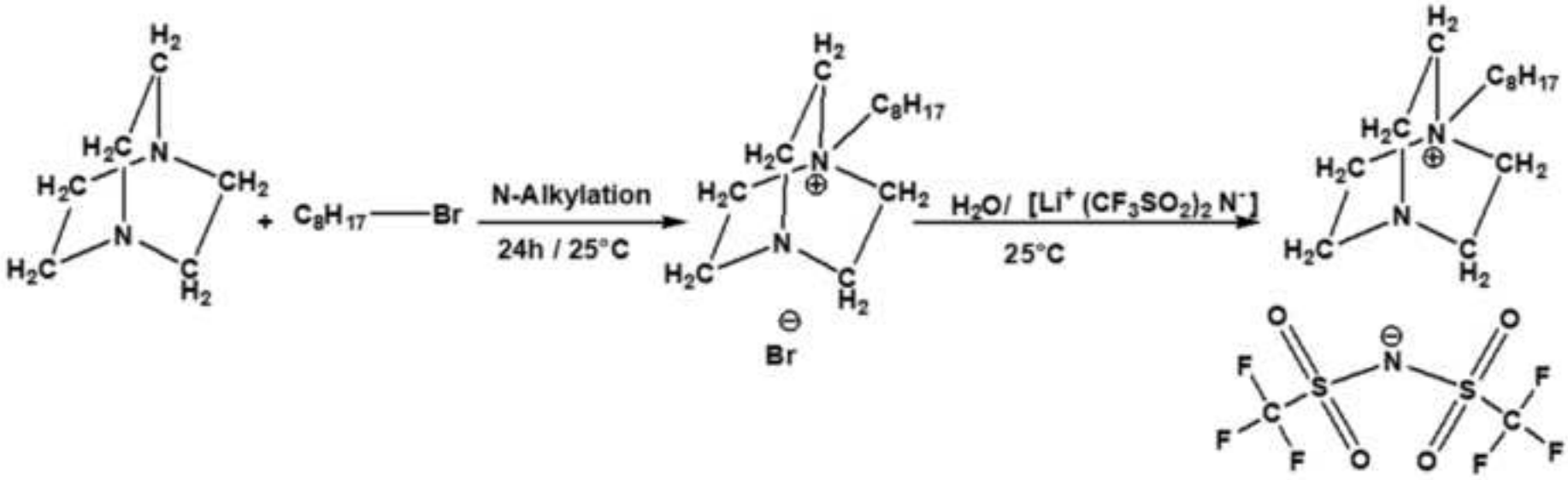

Graphical Abstract

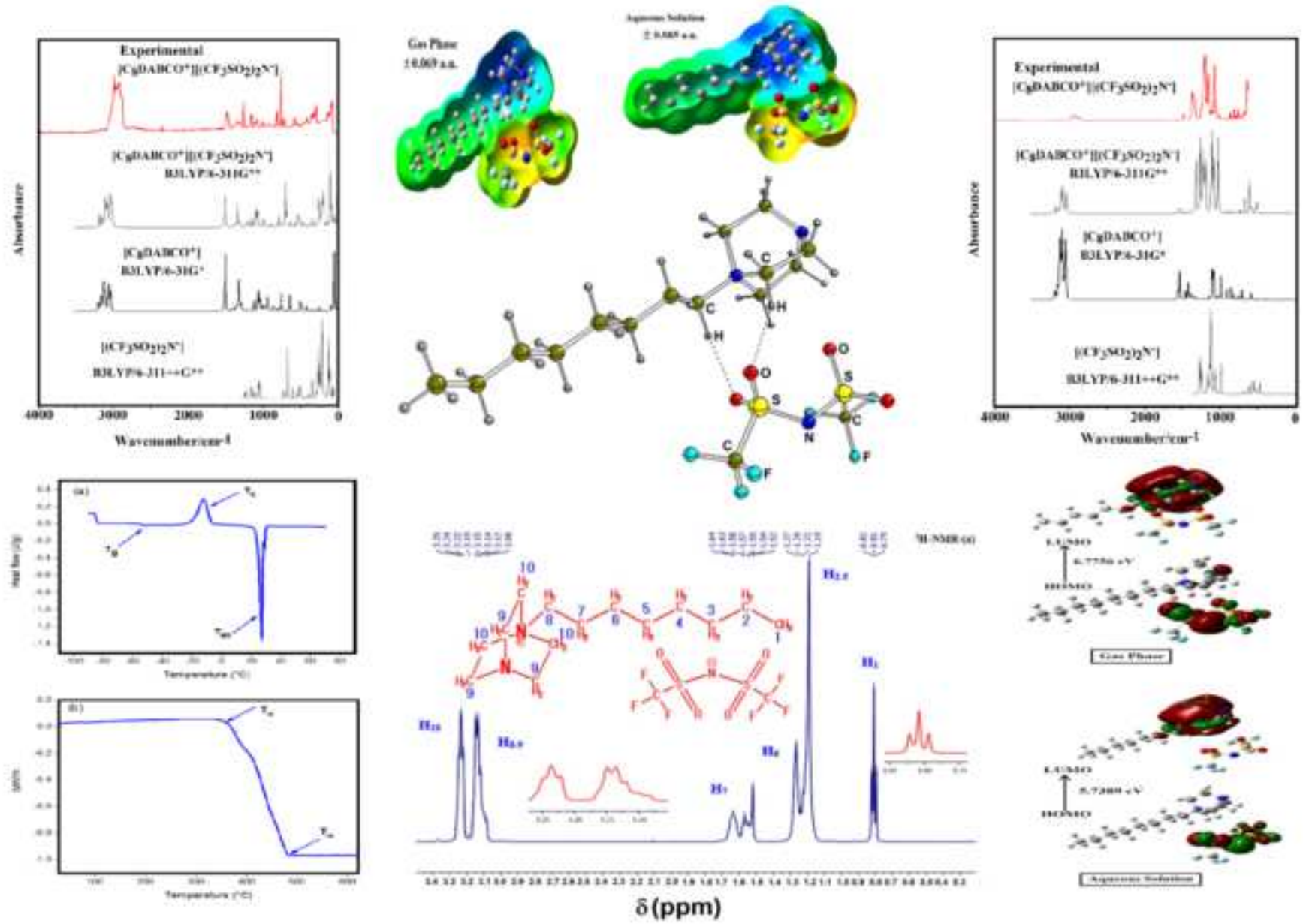

MATERIAL SUPPORTING TO

Synthesis, NMR, IR, Raman spectra and DFT calculations of

1-octyl-1,4-diazabicyclo [2.2.2] octan-1-ium bis(trifluoromethylsulfonyl)imide

Boumediene Haddad[1,2,*], Silvia Antonia Brandán[3],Bekhaled Fetouhi[4,5],Annalisa Paolone[6], Mostefa Boumediene[1], Didier Villemin[2], Mustapha Rahmouni[5], Serge Bresson[7]

[1] Department of Chemistry, Dr. Moulay Tahar University of Saida, 20000 Saida, Algeria.

[2] LCMT, ENSICAEN, UMR 6507 CNRS, University of Caen, 6 bd Ml Juin, 14050 Caen, France

[3] Cátedra de Química General, Instituto de Química Inorgánica, Facultad de Bioquímica. Química y Farmacia, Universidad Nacional de Tucumán, Ayacucho 471, (4000) San Miguel de Tucumán, Tucumán, Argentina

[4]Faculty of Natural and Life Sciences, University of Tiaret, BP78 ZaarouraTiaret 14000, Algeria

[5] Synthesis and Catalysis Laboratory LSCT, Tiaret University, Tiaret, Algeria

[6] CNR-ISC, U.O.S. La Sapienza, Piazzale A. Moro 5, 00185 Roma, Italy

[7]UP Transformations & Agro-Ressources, Institut Polytechnique UniLaSalle, SFR Condorcet 3417, BP 30313, F-60026 Beauvais, France

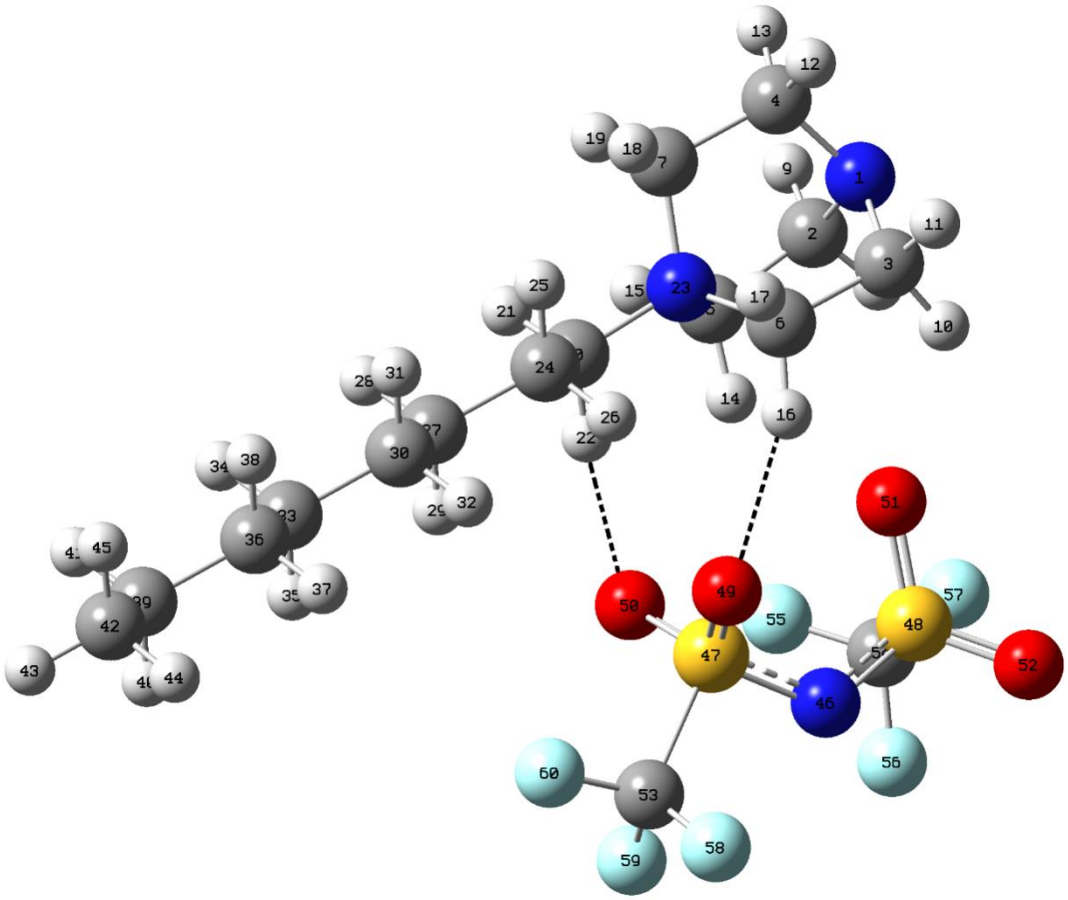

Figure S1. Optimized structure (III) of $[C_8DABCO^+][(CF_3SO_2)_2N^-]$ ionic liquid in gas phase by using the B3LYP/6-311G** level of theory showing the formation of intra-molecular H bonds between the S=O group and the H atoms of CH_2 groups.

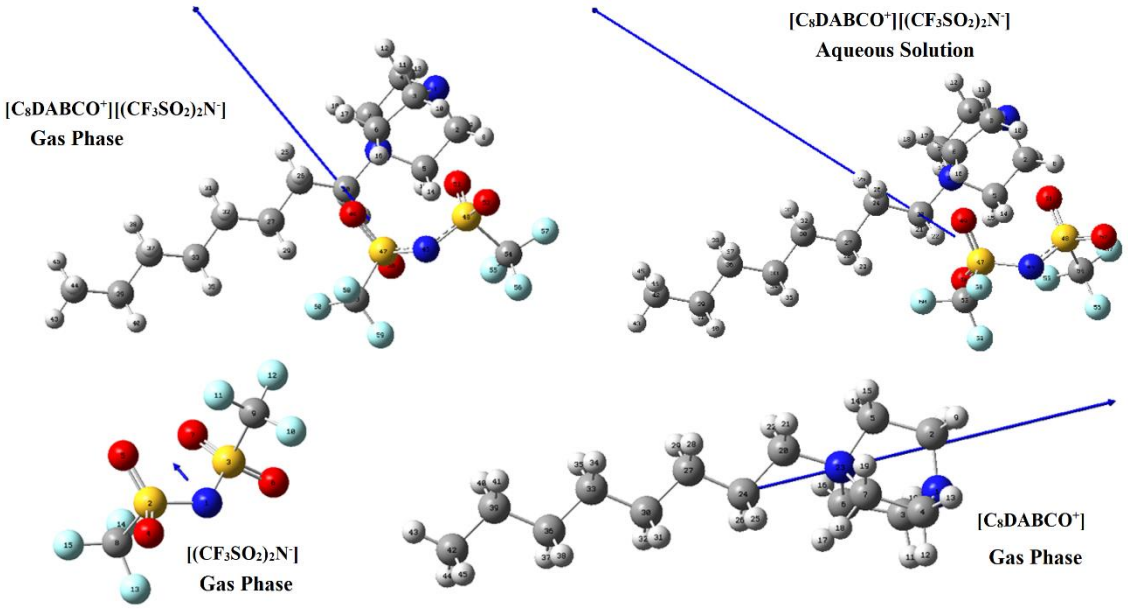

Figure S2. Orientations and directions of dipole moment vectors for $[C_8DABCO^+][(CF_3SO_2)_2N^-]$ IL (upper) in both media and its $[C_8DABCO^+]$ cation and $[(CF_3SO_2)_2N^-]$ anion (bottom) in gas phase by using the B3LYP level of theory and different basis sets.

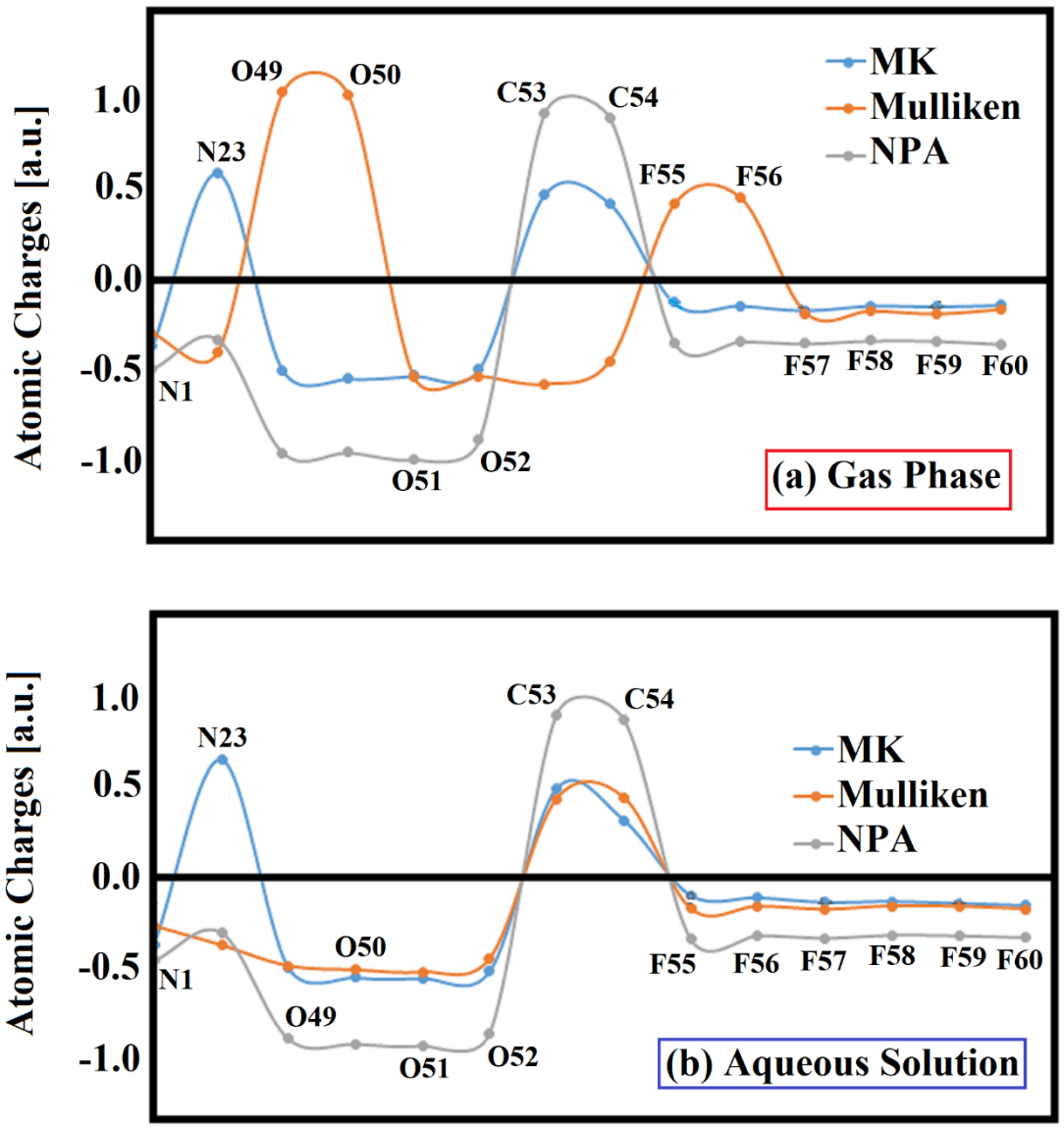

Figure S3. Calculated atomic MK, Mulliken and NPA charges on the N, C53, C54 and F atoms of $[C_8DABCO^+][(CF_3SO_2)_2N^-]$ IL,(a) in gas phase and (b) in aqueous solution by using the B3LYP/6-311G** level of theory.

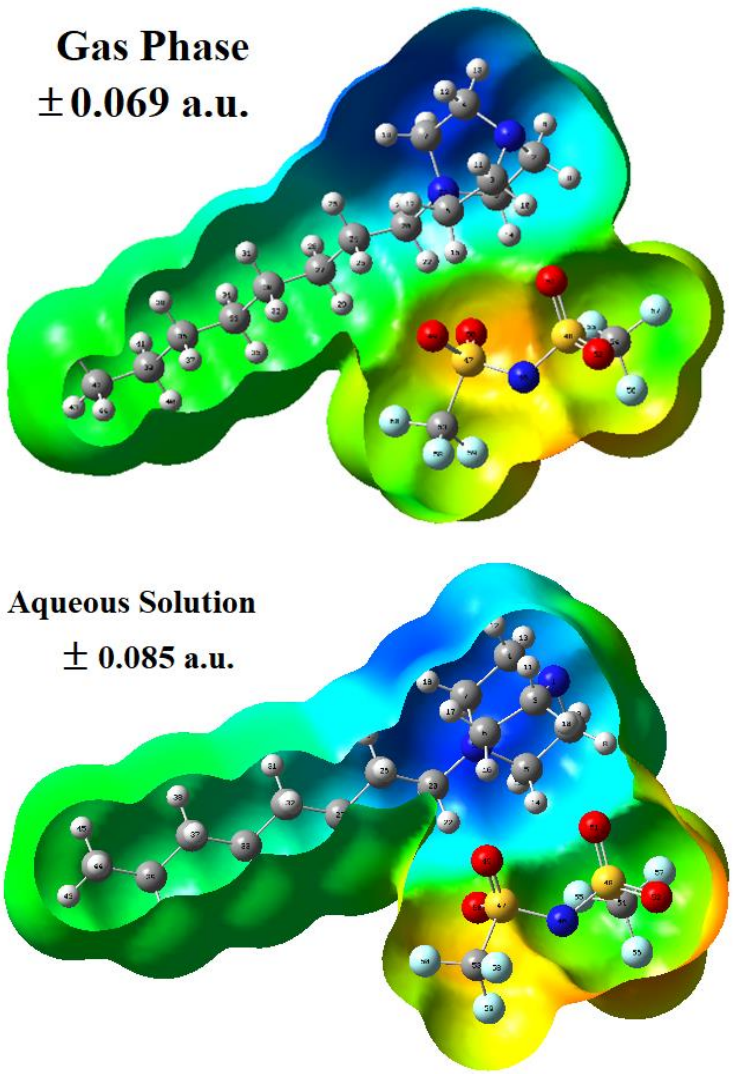

Figure S4. Calculated electrostatic potential surfaces on the molecular surface of $[C_8DABCO^+][(CF_3SO_2)_2N^-]$ IL,(upper) in gas phase and (bottom) in aqueous solution by using the B3LYP/6-311G** level of theory. Iso-density value of 0.005.

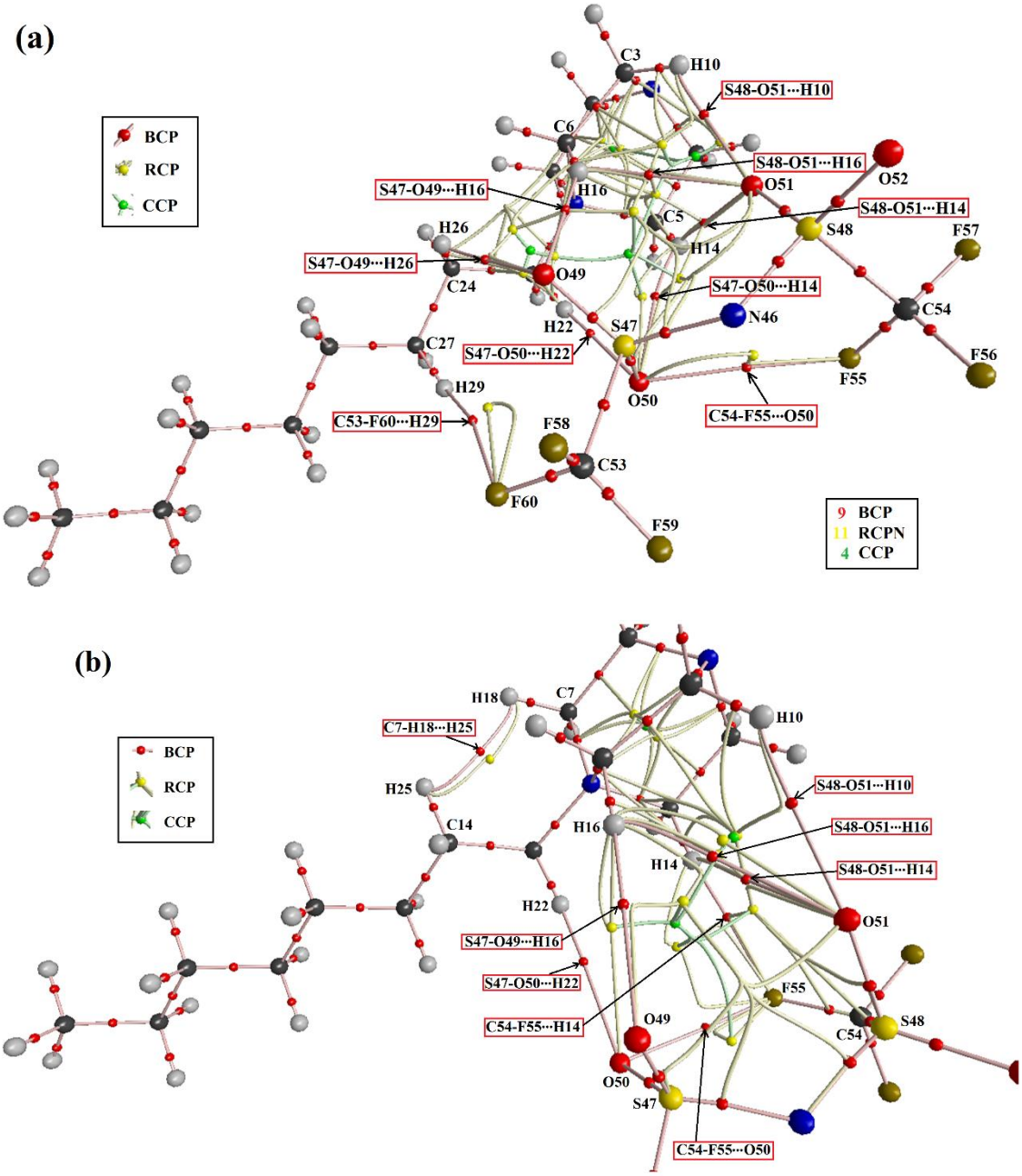

Figure S5. Molecular graphicsfor $[C_8DABCO^+][(CF_3SO_2)_2N^-]$ IL,(a) in gas phase and (b) in aqueous solution by using the B3LYP/6-311G** level of theory.

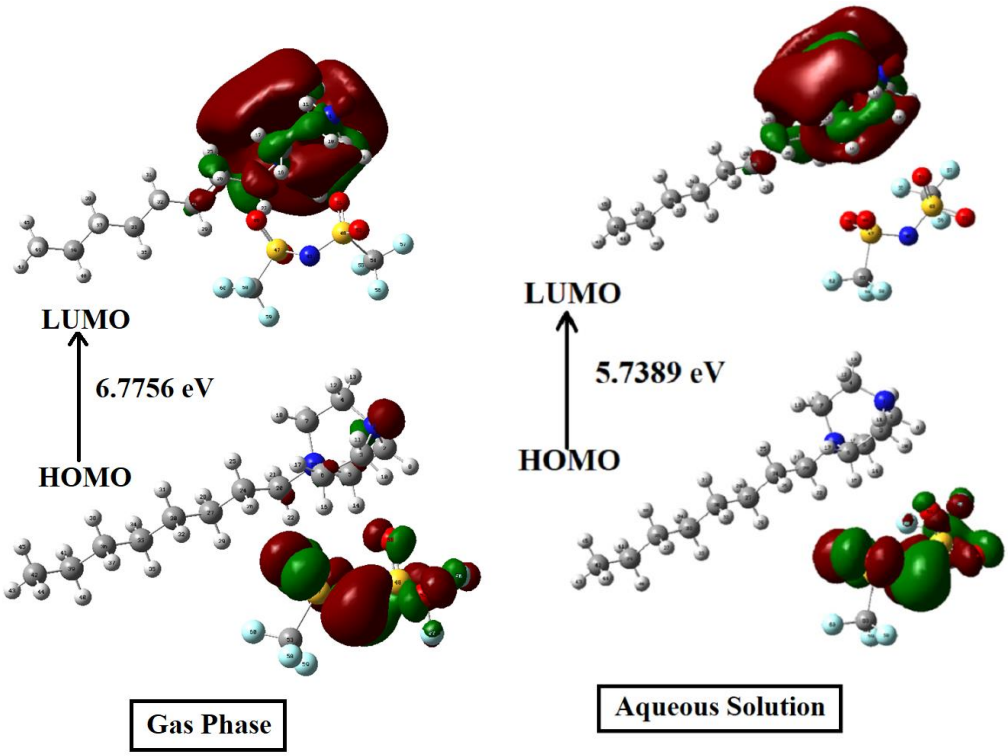

Figure S6. Characteristics of HOMO-LUMO orbitals for $[C_8DABCO^+][(CF_3SO_2)_2N^-]$ IL showing the gap values in gas phase and aqueous solution by using the B3LYP/6-311G** level of theory.

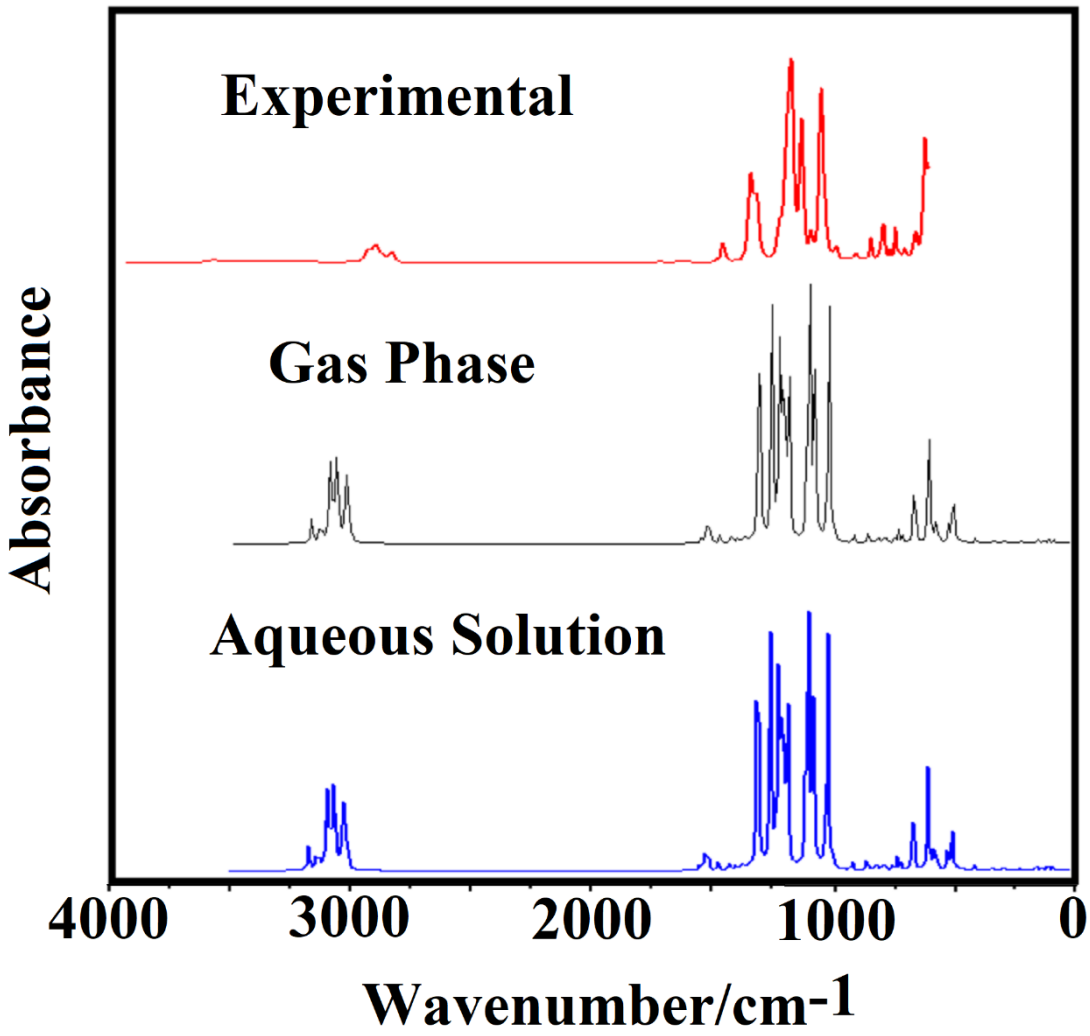

Figure S7. Experimental FT-IR spectrum of ionic liquid in the solid phase compared with the corresponding predicted for IL in gas phase and aqueous solution by using the B3LYP/6-311G** level of theory.

Table S1. Calculated atomic MK, Mulliken and NPA charges on the N, C53, C54 and F atoms of $[C_8DABCO^+][(CF_3SO_2)_2N^-]$ IL in gas phase and in aqueous solution by using the B3LYP/6-311G** level of theory.

B3LYP/6-311G**METHOD						
$[C_8DABCO^+][(CF_3SO_2)_2N^-]$						
Atoms	Gas Phase			AqueousSolution		
	MK	Mulliken	NPA	MK	Mulliken	NPA
1 N	-0.365	-0.294	-0.490	-0.388	-0.285	-0.482
23 N	0.592	-0.398	-0.326	0.658	-0.393	-0.322
49 O	-0.499	1.042	-0.954	-0.518	-0.512	-0.926
50 O	-0.544	1.023	-0.952	-0.576	-0.534	-0.956
51 O	-0.528	-0.535	-0.992	-0.580	-0.547	-0.966
52 O	-0.489	-0.531	-0.883	-0.541	-0.470	-0.895
53 C	0.473	-0.574	0.922	0.495	0.439	0.916
54 C	0.424	-0.445	0.898	0.315	0.446	0.888
55 F	-0.129	0.427	-0.349	-0.111	-0.187	-0.361
56 F	-0.140	0.457	-0.338	-0.123	-0.172	-0.339
57 F	-0.166	-0.182	-0.350	-0.149	-0.190	-0.354
58 F	-0.140	-0.170	-0.334	-0.144	-0.170	-0.337
59 F	-0.145	-0.186	-0.336	-0.155	-0.173	-0.340
60 F	-0.136	-0.161	-0.353	-0.167	-0.188	-0.351

Table S2. Molecular electrostatic potentials (MEP) and Bond orders (BO) expressed as Wiberg bond index, totals by atomfor theN, C53, C54 and F atoms of[C_8DABCO^+][$(CF_3SO_2)_2N^-$] IL in gas phase and in aqueous solution by using the B3LYP/6-311G** level of theory.

Atoms	MEP (a.u.)		Bond Orders	
	Gas	Aqueous Solution	Gas	Aqueous Solution
1 N	-18.365	-18.347	3.114	3.111
23 N	-18.242	-18.220	3.568	3.570
49 O	-22.391	-22.416	1.601	1.636
50 O	-22.391	-22.410	1.604	1.603
51 O	-22.388	-22.409	1.549	1.589
52 O	-22.398	-22.423	1.698	1.674
53 C	-14.505	-14.524	3.655	3.651
54 C	-14.515	-14.524	3.643	3.631
55 F	-26.573	-26.571	1.034	1.020
56 F	-26.575	-26.583	1.050	1.048
57 F	-26.574	-26.576	1.032	1.029
58 F	-26.570	-26.588	1.055	1.051
59 F	-26.569	-26.587	1.052	1.047
60 F	-26.568	-26.583	1.601	1.031

Table S3. Main delocalization energy (in kJ/mol) of $[C_8DABCO^+][(CF_3SO_2)_2N^-]$ IL in gas phase and in aqueous solution by using the B3LYP/6-311G** level of theory.

B3LYP/6-311G** METHOD		
$[C_8DABCO^+][(CF_3SO_2)_2N^-]$		
Delocalization	Gas	PCM
*LP(2)N46→σ*S47-O49*	57.39	
*LP(2)N46→σ*S47-O50*	43.85	54.84
*LP(2)N46→σ*S48-C54*	70.60	77.54
*LP(2)O49→σ*N46-S47*	69.81	71.39
*LP(2)O49→σ*S47-O50*	63.41	66.55
*LP(3)O49→σ*S47-C53*	98.31	102.66
*LP(2)O50→σ*N46-S47*	72.73	73.57
*LP(2)O50→σ*S47-O49*	61.74	59.02
*LP(3)O50→σ*S47-C53*	99.02	98.44
*LP(2)O51→σ*N46-S48*	82.51	87.74
*LP(3)O51→σ*S48-O52*	47.07	51.21
*LP(3)O51→σ*S48-C54*	72.90	77.96
*LP(2)O52→σ*N46-S48*	77.87	76.37
*LP(2)O52→σ*S48-O54*	51.54	
*LP(3)O52→σ*S48-C51*	83.56	71.81
*LP(3)O52→σ*S48-C54*	54.97	64.58
*LP(2)F55→σ*S48-C54*	43.39	0.00
*LP(3)F55→σ*C54-F57*	52.88	44.60
*LP(2)F55→σ*S48-C54*	46.57	
*LP(3)F56→σ*C54-F55*	48.32	49.62
*LP(3)F56→σ*C54-F57*	46.11	45.06
*LP(2)F57→σ*S48-C54*	42.18	
*LP(3)F57→σ*C54-F55*	47.40	51.00
*LP(3)F57→σ*C54-F56*	42.43	
*LP(2)F58→σ*S47-C53*	46.15	47.94
*LP(3)F58→σ*C53-F59*		43.26
*LP(3)F58→σ*C53-F60*	61.20	51.25
*LP(2)F59→σ*S47-C53*	45.60	46.57
*LP(3)F59→σ*C53-F60*	60.90	56.14
*LP(2)F60→σ*S47-C53*		41.93
*LP(3)F60→σ*C53-F58*	42.26	
*LP(3)F60→σ*C53-F59*	45.90	49.45
$\Delta ET_{LP\rightarrow\sigma^*}$	**1778.55**	**1560.48**
*σ*N46-S47→σ*N46-S48*		252.10
*σ*N46-S48→σ*C54-F57*	55.89	
*σ*S48-O51→σ*S48-O52*	72.48	204.65
$\Delta ET_{\sigma^*\rightarrow\sigma^*}$	**128.37**	**456.75**
ΔET_{TOTAL}	**1906.92**	**2017.23**

Table S4. Predicted intramolecular interactions for the $[C_8DABCO^+][(CF_3SO_2)_2N^-]$ ionic liquid in gas phase and aqueous solution by using the topological properties and the B3LYP/6-311G** Method.

Interactions[a]	
Gas Phase	Aqueous solution
S47-O49···H16	S47-O49···H16
S47-O49···H26	
S47-O50···H14	
S47-O50···H22	S47-O50···H22
S48-O51···H10	**S48-O51···H10**
S48-O51···H14	S48-O51···H14
S48-O51···H16	S48-O51···H16
C53-F60···H29	
C54-F55···O50	C54-F55···O50
	C54-F55···H14
	C14-H25···H18

[a]This work; Letters bold, shorter distances.

Table S5. Analysis of the topological properties for the $[C_8DABCO^+][(CF_3SO_2)_2N^-]$ ionic liquid in gas phase and aqueous solution by using the B3LYP/6-311G** Method.

Parameter (a.u.)	Gas Phase		Aqueous Solution	
	S47-O49···H16	S47-O50···H22	S48-O51···H10	C54-F55···H14
$\rho(r_c)$	0.0143	0.0164	0.0038	0.0047
$\nabla^2\rho(r_c)$	0.0471	0.0547	0.0140	0.0187
λ_1	-0.0153	-0.0185	-0.0030	-0.0045
λ_2	-0.0145	-0.0174	-0.0028	-0.0044
λ_3	0.0770	0.0906	0.0197	0.0276
$\lvert\lambda_1\rvert/\lambda_3$				
Distance (Å)	2.261	2.189	2.827	2.654